Characterisation of Intrinsic Firing Properties of Type I Local Interneurons and Uniglomerular Projection Neurons in the Antennal Lobe of the Cockroach *Periplaneta americana*

Bachelor Thesis

Jan Radermacher

October 2014

Gutachter:	Prof. Dr. Peter Kloppenburg
Zweitgutachter:	PD Dr. Joachim Schmidt

Contents

Abbreviations

ADP	afterdepolarisation
AHP	afterhyperpolarisation
Al	antennal lobe
AMPA-receptor	α-amino-3.hydroxy-5-methyl-4-isoxazolepropionic acid receptor
AP	action potential
BK_{Ca}	big conductance K_{Ca} channel
Ca	calyces
Cd	Cadmium
CNQX	6-cyano-7-nitroquinoxaline-2,3-dion
DAP-6	D-2-amino-5-phosphonopentanoic acid
DTX	dentrotoxin
EGTA	ethylene diamine tretraacetic acid
GABA	γ-aminobutteracid
GL	glomeruli
HCN	hyperpolarisation activated cyclic nucleotide-gated channels
HEPES	2-(4-(2(hydroxyethyl)-l-piperazineethanesulfnonic acid
I_A	transient potassium channel
I_h	hyperpolarisation activated current
I_F	I_h
ISF	instantaneous spike frequency

ISI	interspike interval
K_{Ca}	K^+ dependent Ca^+ channel
K_V	voltage gated K^+ channel
LGMD	lobula giant movement detector
LH	lateral horn
mALT	medial antennal lobe tract
MΩ	mega ohm
PBS	phosphate-buffer-system
PIR	post inhibitory rebound
PN	projection neuron
PTX	picrotoxin
R_{inp}	input resistance
RS	series resistant
SD	standard deviation
SEM	standard error of the mean
SFA	spike frequency adaptation
SK_{Ca}	small conductance K_{Ca} channel
TTX	Tetrodotoxin
type I LN	typ I local interneuron
uPN	uniglomerular projection neuron

Abstract

The olfactory system of the cockroach *Periplaneta americana* offers broad opportunities to investigate olfactory information processing. The advantages of the neuronal network of insects are a clear structure, a small number of neurons and the location of the cell bodies in the periphery, which makes them easy accessible for different electrophysiological techniques. Most cellular components have already been identified and described. Nevertheless, the overall knowledge of cell specific computing, encoding and distribution of olfactory information remains fragmentary. In order to extend and broaden our knowledge of insect sensory systems, which are closely related to those of vertebrates, further studies on specific ion channels and their contribution to intrinsic electrophysiological properties are required.

Therefore, cell intrinsic electrophysiological properties of type I local interneurons (type I LN) and uniglomerular projection neurons (uPN) in the antennal lobe of the olfactory system of *Periplaneta americana* were investigated. All experiments were performed in presence of specific synaptic blockers to isolate the cells from synaptic input of other neurons participating in the system. Here, whole-cell patch-clamp recordings in current-clamp mode were the method of choice, which allow detailed recording of steady-state (e.g. resting membrane potential, input resistance and capacitance) and spiking properties.

Although type I LNs were considered to be a homogenous cell population, the results of this thesis indicate a more heterogeneous group with regard of their electrophysiological properties. Based on their specific spike frequency modulations in response to depolarisating current injections type I LNs form three subpopulations. Although all type I LNs showed spike frequency adaptation (SFA), they showed different grades of SFA. Thus, strong and weak adapting type I LNs formed two different subpopulations. In response to longer stimuli a third population of diphasic adapting neurons with SFA in the first part and an acceleration of spike frequency in the second part of the stimuli. These findings indicate that not only the amount of current but also the duration of stimuli is frequency coded. All recorded uPNs showed a homogenous spike frequency pattern in response to depolarisating stimuli. Here, continuous spike frequency acceleration was observed. The mentioned adaptation modulations indicate strong differences in number and composition of ion currents in the cells. Subthreshold

stimulations of LNs revealed a depolarising voltage hump at the beginning of the pulses that might contribute to SFA since duration of the hump and of the phase of strongest adaptation were overlapping. In contrast, subthreshold stimulations of uPNs showed a sustaining voltage ramp, which also might contribute to the sustaining frequency acceleration of the recorded neurons.

Additionally, cell respondings to hyperpolarising current injections revealed that both type I LNs and uPNs developed a sag-potential driven by a Na^+-influx through hyperpolarisation activated currents (I_h). In contrast, the responses differed in terms of post inhibitory rebound (PIR) properties: While type I LNs showed PIR related firing at the offset of negative stimuli, uPNs did not. Here, both differences in current sensitivity to negative voltages and differences in number and composition might be responsible.

Zusammenfassung

Das olfaktorische System der Schabe *Periplaneta americana* bietet vielfältige Möglichkeiten um die Prozessierung von olfactorischen Informationen zu untersuchen. Die Vorteile dieses Systems liegen in der klaren Strukturierung, der geringen Anzahl von Neuronen und der peripheren Lage der Zellkörper, wodurch diese für elektrophysiologische Methoden einfach zugänglich sind. Die meisten zellulären Bestandteile wurden bereits identifiziert und charakterisiert. Dennoch ist unser Wissen über die zellspezifische Verarbeitung, Kodierung und Verteilung/Organisation von olfaktorischen Informationen noch lückenhaft. Um unser Wissen über sensorische Systeme der Insekten, die viele Parallelen zu denen von Vertebraten aufweisen, zu vervollständigen, müssen detaillierte Experimente zu spezifischen Ionenkanälen und deren Rolle für die zell-intrinsischen elektrophysiologischen Eigenschaften durchgeführt werden.

Zu diesem Zweck wurden die zellintrinsischen elektrophysiologischen Eigenschaften von Typ I lokalen Interneuronen (Typ I LN) und uniglomerulären Projektionsneuronen (uPN) im Antennallobus (AL) von *Periplaneta americana* untersucht. Alle Experimente wurden an synaptisch isolierten Zellen in Form von *patch-clamp* Ableitungen in der *current-clamp* Konfiguration, durchgeführt. Diese Messtechnik ermöglicht detaillierte Untersuchungen von wesentlichen Ruhemembraneigentschaften, wie z.B. das Ruhemembranpotential, Eingangswiederstände und Zellkapazität, und Aktionspotentialeigenschaften.

Typ I LNs wurden als eine homogene Neuronenpopulation betrachtet, jedoch zeigen die Ergebnisse dieser Arbeit, dass es sich in Bezug auf die spezifischen elektrophysiologischen Eigenschaften um eine heterogene Population handelt. Hier wurde gezeigt, dass Typ I LNs unterschiedliche Muster von Spike-Frequenzadaptation (SFA) in Antwort auf depolarisierende Strominjektionen generierten und danach unterteilt werden können. So wurden zunächst stark und schwach adaptierende Typ I LNs gefunden. In Antwort auf länger andauernde Depolarisation konnte eine dritte Gruppe von diphasisch adaptierender Neurone gefunden werden, die noch zu Anfang der Stimulation SFA zeigten, aber im weiteren Verlauf der Stimulation eine Zunahme der Aktionspotentialfrequenz beschrieben.

Dies deutet darauf hin, dass nicht nur die Stärke, sondern auch die Dauer einer Stimulation dieser Neurone frequenz-codiert wird.

Alle abgeleiteten uPNs zeigten eine Beschleunigung der Spike-Frequenz in Antwort auf einen depolarisierenden Stimulus und konnten in diesem Punkt als einheitliche Gruppe bestätigt werden.

Die unterschiedlichen Frequenzmodulationen deuten darauf hin, dass Typ I LNs und uPNs große Unterschiede in der Anzahl und Komposition von Ionen- Kanälen aufweisen.

Eine unterschwellige Stimulation der Typ I LNs zeigte eine stark depolarisierende Flanke zum Beginn des Stimulus, welche an der beschrieben SFA beteiligt sein könnte: die Dauer der beobachteten zusätzlichen Depolarisation überschnitt sich mit der der höchsten Frequenz dieser Neurone. Auch uPNs wurden unterschwellig stimuliert, wobei eine kontinuierliche Depolarisation des Membranpotentials beobachtet werden konnte. Dieser Effekt könnte eine Ursache für die Frequenzbeschleunigung dieser Neurone darstellen.

Zusätzlich wurde untersucht, wie die Zellen auf hyperpolarisierende Strominjektionen reagierten: Hierbei zeigten sowohl Type I LNs als auch uPNs die Ausbildung eines depolarisierenden sag-Potentials durch einen Na^+ Einstrom durch hyperpolraisations-aktivierte Kanäle (I_h). Im Gegensatz dazu unterschieden sich beide Zelltypen in Bezug auf den Effekt des *postinhibitorischen rebound* (PIR). Während Typ I LNs ein PIR assoziiertes Feuern von Aktionspotenzialen zeigten, konnte in uPNs eine solche Reaktion nicht festgestellt werden. Dies weist darauf hin, dass Unterschiede in der Sensitivität von Kanälen auf negative Spannungen, aber auch generelle Unterschiede in Anzahl und Komposition der Kanäle vorliegen könnten.

1 | Introduction

The ability to perceive and process complex odour information provided a significant evolutionary way of communication. Complex neural circuits formed the insect olfactory system to a remarkably efficient neuronal network. The insect antennal lobe (AL) is considered as the analogue to the olfactory bulb of vertebrates, suggesting that the underlying mechanism of processing olfactory information and the required anatomical organization is ecolutionary conserved among different taxa. The AL is the first synaptic relay for the olfactory information processing (Davis 2004; Hildebrand & Shepherd 1997; Ito et al. 2014; Strausfeld & Hildebrand 1999). The variety of glomeruli strongly differs between different species and especially different taxa. The number of glomeruli in insect olfactory system varies between 50– 300, whereas mice as representatives of mammals possess approximately 1000 glomeruli. Since the AL of *Periplaneta americana* only consists of 124 ordinary and 1 gender specific glomeruli, which detects female specific pheromones (Hildebrand & Shepherd 1997), the olfactory is small and clearly structured (Ernst et al. 1977). Furthermore, the cell bodies of different neuron types are located in the periphery which makes them easily accessible for electrophysiological techniques. Thus, the cockroach olfactory system is a good model organism to investigate the complex processing of olfactory information. Although the insect olfactory system has been studied intensively (Boeckh & Ernst 1987; Christensen et al. 1993; Davis 2004; Ernst et al. 1977; P Kloppenburg, Kirchhof, et al. 1999; Peter Kloppenburg et al. 1999; Strausfeld & Hildebrand 1999), our knowledge of cell specific processing of olfactory information and the underlying cell intrinsic electrophysiological properties is still fragmentary.

1.1 The olfactory system of the cockroach

Detection of olfactory information takes place in the sensillae of the antennae by olfactory receptor neurons (ORN) each expressing a single receptor gene (Hildebrand & Shepherd 1997), projecting via their axons to the AL. In the AL, the axons of those ORNs expressing the same receptor gene converge onto the same specific glomerulus (Davis 2004; Vosshall et al. 2000). The antennal nerve has been shown to contain approximately 80.000 axons of ORNs (Ernst et al. 1977). In the glomeruli, ORNs form divergent synapses with uniglomerular projection neurons (uPN) and local interneurons (LN) (Figure 1).

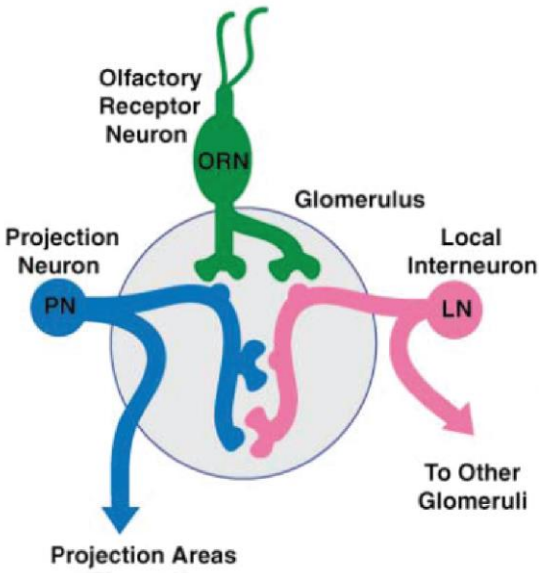

Figure 1: Schematic overview of synaptic connections in a glomerulus of the antennal lobe (from Davis, 2004).

Olfactory receptor neuros (ORN) innervate local interneurons (LN) and projection neurons (PN) within a specific glomerulus.

LNs were shown to mediate complex interactions between different glomeruli by forming multiglumerular ramifications within the whole antennal lobe (Sun et al. 1997), primarily as GABAergic inhibitory neurons. Furthermore, LNs are known to exhibit reciprocal dendrodentritics connections to PNs serving as transmissive and receptive junctions, suggesting, that single glomeruli make computations underlying odor perception, discrimination and learning but not only serving as transit stations for olfactory information (Davis 2004). In contrast, uniglomerular projection neurons (uPNs) in contrast are characterized by a restricted ramification within a single glomerulus in the AL and a long axon to higher-order neuropiles in the protocerebrum (Sun et al. 1997). Here uPNs relay olfactory information in the lateral lobes and the mushroom bodies (Figure 2).

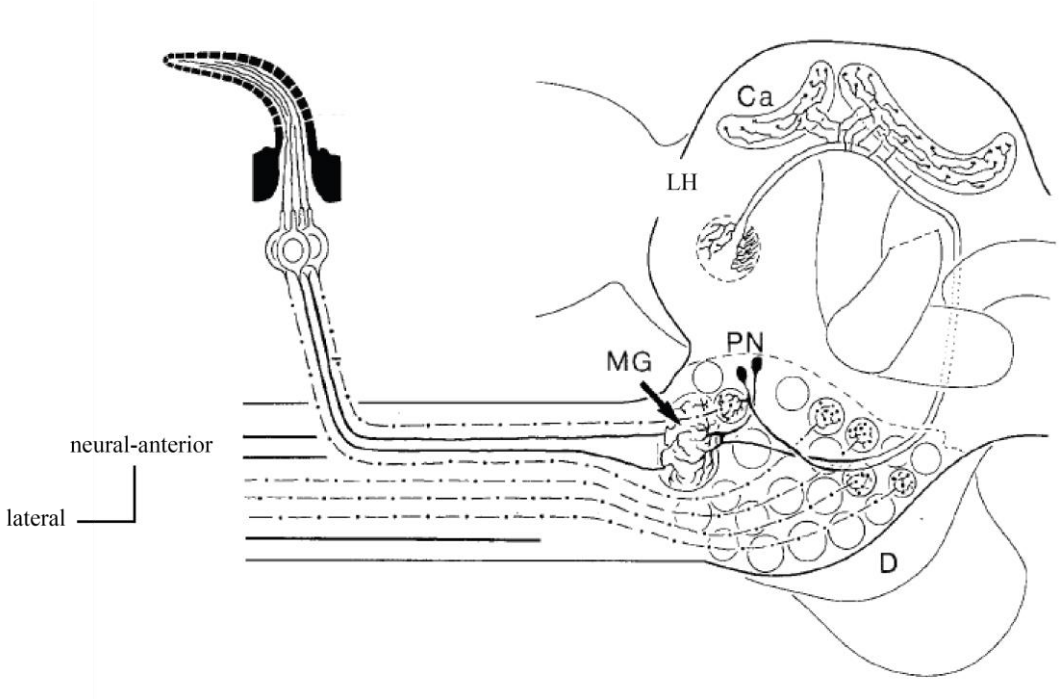

Figure 2: Schematic overview of the olfactory system in the cockroach *Periplaneta americana* (modified from Boeckh and Ernst, 1987).

AN: antennal nerve; Ca: calyces of corpus pendiculatum, D: deutocerebrum, LH: lateral horn, MG: macroglumerular complex, ORN: olfactory receptor neuron, PN: projection neuron, Se: sensilla.

Generally, local interneurons were shown to be a heterogeneous population in regarding to morphology and electrophysiology (Husch et al. 2009a; A. Husch et al. 2009b). The innervation pattern of glomeruli differs among the LN population as well as their possibility to elicit Na^+ driven action potentials. At least two different types of LNs could be classified: Type I LNs are able to generate Na^+ driven action potentials. They are known be GABAergic and therefore put synaptic inhibition on uPNs (Wilson & Laurent 2005). However LNs do not exclusively inhibit uPNs. Temporal patterns of inhabitation followed by excitation seem to encode odour stimulations (Stopfer et al. 1997; Shang et al. 2007). Type I LNs innervate many but not all glomeruli in different densities. The second group of LNs are referred to as "non-spikers" due to the fact that they do not have Na^+ currents required to elicit APs. The type II LNs are further divided in type II a and type II b as the differ in their morphology and Ca^{2+} currents (A. Husch et al. 2009a). Type II a LNs have strong Ca^{2+} dependent membrane properties and in some cases respond to stimulations with Ca^{2+} driven spiklets. They innervate homogenously all glomeruli in AL. Type II b LNs respond with smooth and sustained membrane depolarisations and innervate all glomeruli but only partial.

1.2 Objectives of this thesis

Previous studies einverstigated the contribution of different ion currents to the intrinsic electrophysiological properties of type I LNs and uPNs Although, a detailed characterisation of the intrinsic firing properties of these neurons is still fragmented. The aims of this thesis are to describe cell intrinsic properties of type I LNs and uPNs in the antennal lobe of *Periplaneta Americana.* Here, the focus was set onto the following properties:

1. Spike frequency modulation in response to depolarising stimuli.
2. Shape of action potentials evoked by the stimuli.
3. Cell intrinsic responses to hyperpolarising current injections.

2 | Materials and Methods

2.1 Animals and materials

American cockroaches (*Periplaneta americana*) were kept in a dedicated room and breed under strict conditions. Room temperature was constantly held at 27°C and light conditions were adapted to a 13:11 hour light/dark cycle. Animals had permanent access to dry rodent food, oat flakes and with fresh water. All experiments were performed using adult males with intact antennae. If not stated otherwise, all chemicals were obtained from Sigma-Aldrich (Taufkirchen, Germany) or Applichem (Darmstadt, Germany). Purity grade of used compounds was 'per analysis'.

2.2 Intact brain preparation

To perform electrophysiological experiments on the cockroach antennal lobe neurons, the intact brain preparation was based on an approach described previously (P Kloppenburg, Ferns, et al. 1999; P Kloppenburg, Kirchhof, et al. 1999). The main advantage of this approach is the integrity of the olfactory network. Animals were anesthetized by CO_2 application and firmly secured within its custom built holder. The head was fixed with tape (tesa ExtraPower Gewebeband, Tesa, Hamburg, Germany) and the antennae were cut at the first distal segment. The brain was dissected from the head capsule in normal extracellular saline (referred to as “normal saline”) containing (in mM): 185 NaCl, 4 KCl, 6 $CaCl_2$, 2 $MgCl_2$, 10 HEPES 35 D-glucose adjusted to pH 7.2 using NaOH and to an osmolarity of 430 mOsm with glucose. To remove the capsule two big incisions along the bases of the antennae and between the two compound eyes were made. The further dissection of the brain and its antennal nerves was performed in a Sylgard-coated (Dow Corning Corp., Midland, Michigan, USA) recording chamber. The chamber was constantly filled with normal saline and the brain

was pinned to the Sylgard-coated recording chamber. Using fine forceps the neuronal sheath was removed from the AL, thereby granting access to the neurons and facilitating the penetration of pharmacological agents. Brain preparations were treated with an enzyme mixture containing: 0.3 mg ml^{-1}, P4762, Sigma and L-cysteine 1 mg ml^{-1}, 30090, Fluka/Sigma, both dissolved in "normal saline", for ~2-3 minutes at RT.

2.3 Whole cell recordings

All recordings were performed under visual control using a fixed-stage upright microscope (BX51WI, Olympus) using a 40x waterimmersion objective [UMPLFL, 40, 0.8 numerical aperture (NA), 3.3 mm working distance, Olympus]. Whole cell recordings in current-clamp mode were performed at 24 °C, following the method described by Hamill et al. (1981). To guarantee constant results borosilicate glass (0.86 mm ID, 1.5 mm OD, GB150-8P, Science Products, Hofheim, Germany) electrodes were pulled by a temperature controlled pipette puller (PP-830, Narishige Group, Japan) with a tip resistance of 3-3.5 MΩ. For the following experiments, these electrodes were tip filled with intracellular saline containing (in mM): 190 K-aspartate, 10 NaCl, 1 CaCl2, 2 MgCl2, 10 HEPES and 10 EGTA adjusted to pH 7.2 with KOH, resulting in an osmolality of ~ 415 mOsm. For single cell labelling 1% biocytin (B4261, Sigma) was added to the backfill containing intracellular saline. If not stated otherwise, brains were super fused with normal extracellular saline containing specific synaptic blockers (see 2.4 Synaptic blockers).

Current-clamp whole cell experiments were recorded with an EPC9 amplifier (HEKA-Elektronik, Lambrecht, Germany). PatchMaster (version 2x53, 06 May 2010, HEKA-Elektronik) was used as recording software running on a Windows computer. Sample frequency was set at 10 kHz. Recorded signal was low pass filtered at 2.9 kHz with a bessel-filter. In order to compensate offset potentials and capactitive currents, the "automatic mode" of the EPC9 was used. The whole cell capacitance was manually compensated by the 'c-slow' capacitance compensation function of the EPC9. The calculated liquid junction potential (lq) between the extracellular and intracellular saline was also compensated (15,9 mV, calculated with Patcher's-Power-Tools plug-in from

http://www.mpibpc.gwdg.de/abteilungen/140/software/index.html for Igor Pro [Wavemetrics, Portland, Oregon]). Additionally, voltage discrepancies due to series resistance (RS) were addressed by the EPC9´s RS-compensation. RS compensation was set at 66% with a corresponding time constant (τ) of 10µs.

After the compensation process was done in voltage-clamp mode, the following recordings of the neurons were performed in current-clamp mode. To guarantee comparable results, cells were held at a membrane potential of -60 mV for type I LNs or -70 mV for uPNs respectively. Switching from voltage clamp mode to current clamp mode lead to a deactivation of the RS compensation. Therefore the bridge compensation was enabled and adjusted to 66% (HEKA PatchMaster Manual 2.5, page 346).

2.4 Synaptic Blockers

Since the cell intrinsic firing properties of type I LNs and uPNs were analyse, all brains were super fused with normal saline containing a composition of different specific synaptic blockers of following concentrations: 10 µm CNQX (6-cyano-7-nitroquinoxaline-2,3-dion, Sigma), 50 µm D-AP5 (D-2-amino-5-phosphonopentanoic acid, Sigma), 100 µm PTX (Picrotoxin, Sigma) and 50 µm Tubocurarine (Sigma). CNQX, D-AP5 and PTX block excitatory and inhibitory neurotransmission via AMPA/kainite receptors, NMDA receptors and $GABA_A$ receptors, respectively. Tubocurarine is an antagonist of nicotinic acetylcholine receptors and therefor blocks excitatory input. During the experiments, 10 µm CGP-56426 (Biotrend) was additional used to block inhibitory input via $GABA_B$. Due to new results during the thesis, Tubocurarine was replaced by 100 µm Mecamylamine (Biotrend).

2.5 Data analysis

Acquired electrophysiological data was analysed with the following softwares: Spike2 (version 7.08 for Windows, Cambridge Electronic Design, http://www.ced.co.uk/upu.shtml), Igor Pro 6 (Wavemetrics, including the Patcher's

PowerTools plug-in) and Graphpad5 (version 5.04, Graphpad Software Analyse, Graph and Organize Your Date http://www.graphpad.com/welcome.htm). All calculated values are given as mean ± standard deviation of mean (SD). Significance of differences between mean values was evaluated with one-way-ANOVA and the Newman-Keuls post-test with a p - value ≤ 0.05 for significance.

2.6 Measurement and analysis of cell properties

Resting membrane potential was measured during a period of zero current injection.

Membrane resistance was determined by OHM´s law (Eq. 1). To calculate membrane resistance according to Ohm´s law small hyperpolarising current injections were performed. Voltage was calculated by the subtraction of voltage at the membrane capacity onset and the maximum deflection after hyperpolarisation.

$$I_R = \frac{V_m - E_m}{R_{inp}} \leftrightarrow R_m = \frac{V_M - E_m}{I_R}$$

Equation 1: OHM´s law.
I_R, current through ion channels; V_m, voltage of membrane; E_m, steady state voltage.

Instantaneous spike frequency (ISF) was calculated over a 2.5 s, respectively 6 s depolarizing current injections according to equation 2.

$$ISF = \frac{1}{ISI}$$

Equation 2: Calculation of instantaneous spike frequency (ISF)
ISI, interspike interval.

The spike frequency adaptation (SFA) ratio was calculated using the initial and final ISF of 2.5s and 6 s depolarisating current injections. Therby the initial ISF was calculated using the first AP doublet and the final ISF was calculated using the final AP doublet of the current injection.

The spike frequency adaptation (SFA) ratio was calculated as the instantaneous frequency ratio of the initial AP doublet to the final AP doublet in a spike train.

$$SFA\ ratio = \frac{initial\ ISF}{final\ ISF}$$

Equation 3: Calculation of spike frequency ratio. ISF, instantaneous spike frequency; SFA, spike frequency adaptation.

Firing threshold was determined by the maximum value of second derivative of an averaged action potential.

The spike form was analysed based on the first spike of a spike train. A sweep with a mean instantaneous spike frequency of ~11 Hz (uPN) and ~6 Hz (LN I) was used to get comparable results within the populations.

The amplitude of APs (mV) was determined as the voltage difference between the threshold potential and the APs peak. Action potentials width (ms) was measured at the half maximum of voltage difference between threshold and action potential peak. The afterhyperpolarisation (AHP) (mV) was determined as the voltage difference between the threshold and the lowest peak of AP. The maximal rate of repolarisation (mV/s) was defined as the maximum negative deflection of the first derivative of an average action potential. The fast afterdepolarisation (ADP) (mV) of type I LNs only, was measured as the voltage difference between the peak of AHP and the peak of depolarisation before coming steady stage potential between the analysed and the following AP.

The membrane potential first revealing a sag potential was determined as the plateau potential at the end of the hyperpolarising current injection.

2.7 Single cell labelling and image processing

After the electrophysiological experiments, a long lasting hyperpolarising current was injected to fill the neuron with biocytin from the recording pipette. Brains were unpinned and fixed in Roti-Histofix (P0873, Carl Roth, Karlsruhe, Germany) overnight at 4 °C. The following day, brains were rinsed (3 x 10 min) in 0.1 M Tris-HCl buffered solution (PBS; pH 7.2). To improve the streptavidin penetration, brains were treated with an enzyme mixture containing collagenase/dispase (1 mg ml^{-1} [269638, Roche Diagnostics, Mannheim, Germany) and hyaluronidase (1 mg ml^{-1} [H3506, Sigma-Aldrich]) diluted in PBS. Brain was exposed to this cocktail for 20 minutes at 37°C and afterwards rinsed in PBS (3 x 10 min, 4 °C). To prevent unspecific dye binding the brains were incubated in PBS containing 1% Triton X-100 (Serva, Heidelberg, Germany) and 10% normal goat serum (Linaris GmbH, Wertheim, Germany) for 40 minutes at RT and afterwards rinsed in PBS (3 x 10 min). Afterwards, brains were incubated with 10% normal goat serum and streptavidin conjugated Alexa 633 (1:500, 1 day, 4°C, S21375, Molecular Probes, Eugene, OR, USA) and rinsed in PBS (4 x 10 min). Brains were dehydrated in an ascending ethanol series (50%, 70%, 2x 90%, 2x 100% for 10 min.) In the last step brains were cleared and whole mounted in Methylsalicylate (M6752, Sigma-Aldrich).

Images of the whole mount preparations were taken with an LSM 510 Meta confocal laser scanning system (Carl Zeiss, Jena, Germany), using a Plan-Neufluar 10x (0,3 NA) objectives. Streptavidin-Alexa 633 was excited at 633 nm and emission was collected with a 650 nm low pass filter.

3 | Results

3.1 Identification and morphology of type I LNs and uPNs

Whole-cell patch-clamp recordings were performed on type I LNs and uPNs in the ventrolateral somata group (VSG) of the AL. Both neuron types can be distinguished by the position of their somata in the VSG, their cell morphology and their electrophysiological properties. The somata of the uPNs and type I/II LNs form three distinct clusters within the VSG: the uPN cluster is located on the most ventral surface of the AL and their somata are the smallest of the three cell-types with a diameter of 10-17 µm. Dorsaly located to the uPN cluster lie the type I LNs with a somata diameter of 20-40 µm. Type II LNs somata are located most dorsaly in the VSG. Their somata have diameters of 50-80µm.

Furthermore, these AL neurons can also be identified by their electrophysiological properties. Since type II LNs don not express voltage dependent Na^+-channels and thus are not able to generate Na^+-driven action potentials upon current injection or odour stimulation, they only respond to stimuli with a graded depolarisation (Husch et al. 2009a,b). In contrast, type I LNs and uPNs express voltage dependent Na^+-channels and respond to the stimuli with Na^+-driven action potentials.

Single cell labelling with biocytin and subsequent Alexa Fluor 633 streptavidin binding allowed the distinct identification of the recorded neuron types. The morphologies of a representative uPN and type I LN are shown in Figure 3 and Figure 4.

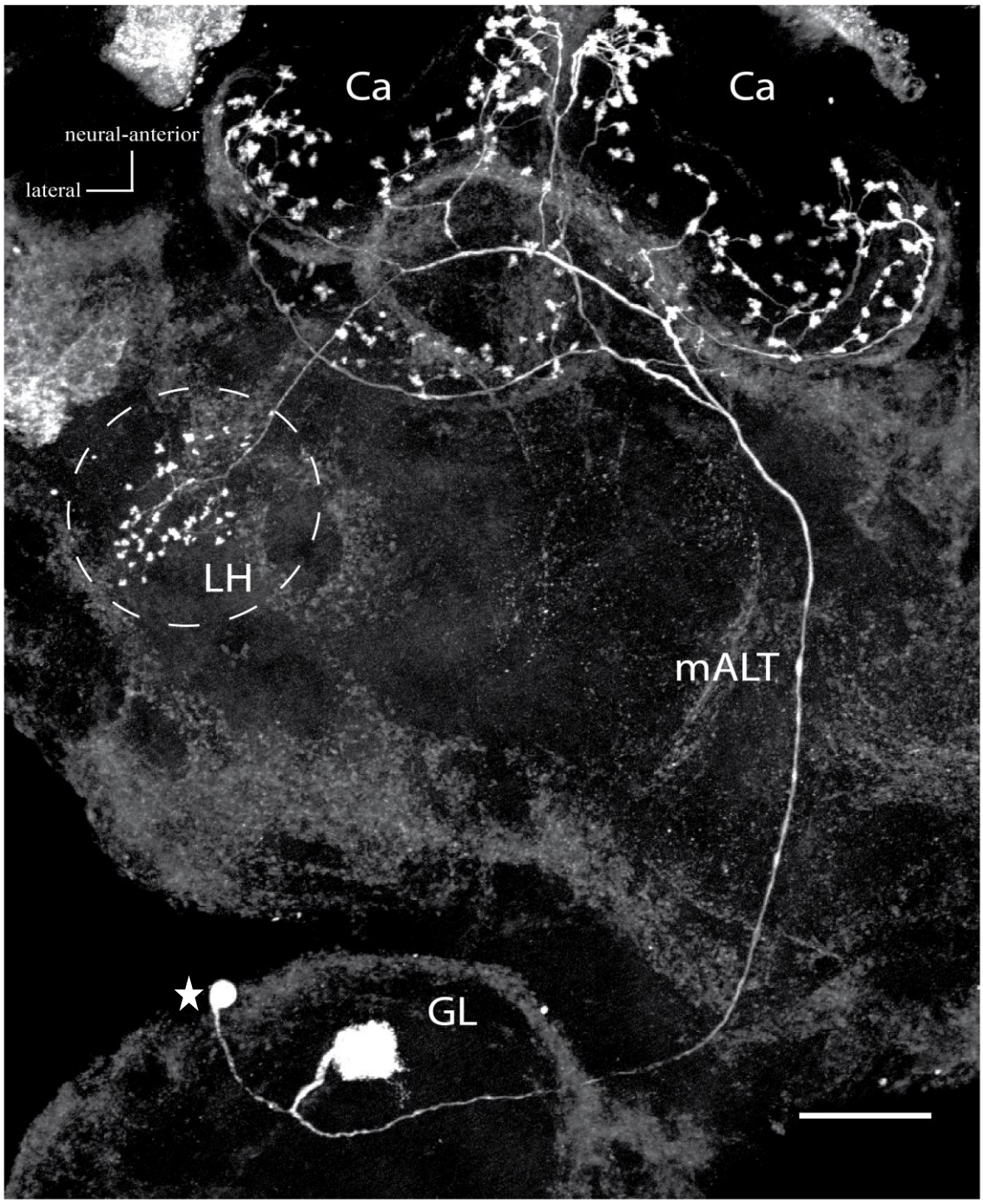

Figure 3: Morphology of a biocytin/Alexa Fluor 633 streptavidin labelled uPN.

Maximum intensity Z-projection of a confocal image stack of a biocytin/streptavidin staining. The soma is marked by a star. In the antennal lobe, the uPNs neurites only innervate a single glomerulus. The axon projects through the medial antennal lobe tract to the protocerebrum to innervate the mushroom body calyces and the lateral horn. Scale bar: 100 µm. Ca: calyces; GL: antennal lobe glomerulus; LH: lateral horn; mALT: medial antennal lobe tract.

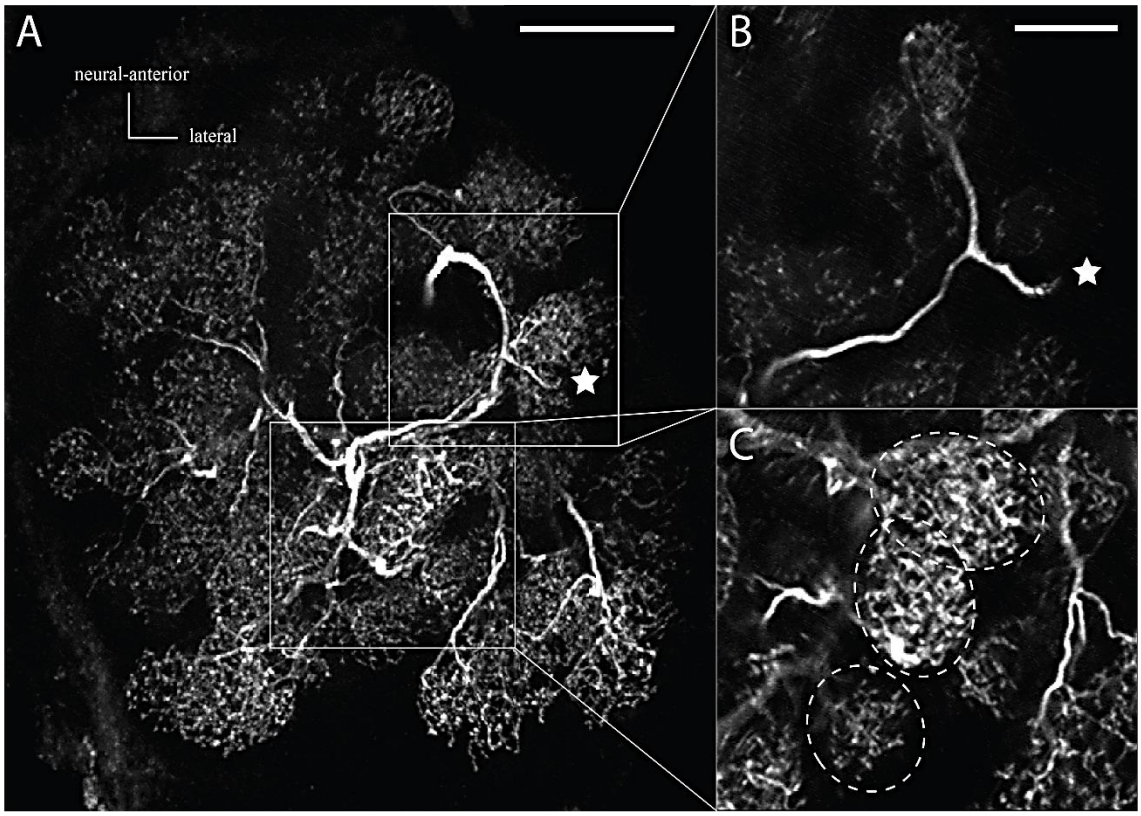

Figure 4: Morphology of a biocytin/Alexa Fluor 633 streptavidin labelled type I LN.
(A) Maximum intensity Z-projection of a confocal image stack of a biocytin/streptavidin staining. Cell body was lost due to mechanical forces during processing (asterisk indicates the position of the cell body). Scale bar: 100 µm. Branching pattern is restricted to the antennal lobe. ***(B)*** Enlarged section of the characteristic y-shaped tract of the type I LNs. Scale bar: 50 µm. ***(C)*** Enlarged section of glomeruli (dashed lines) that are innervated with different densities. Scale bar: 50 µm.

3.2 Current-clamp experiments

All recordings were performed in whole cell configuration, in the current-clamp mode. To investigate the intrinsic firing properties of type I LNs and uPNs, four current-clamp protocols were designed (Figure 5). Protocol C (Figure 5, C), consisting of hyperpolarising current injections, was applied to determine input resistance (R_{inp}). Therefore, this protocol was applied ~5 min after getting access to the intracellular compartment of the cell. Using protocol A (Figure 5, A) positive current steps were injected that depolarised the cell to induce action potentials. Thus, spike threshold could be determined. The respective current amount served as reference for protocol B

(Figure 5, B). Here, increasing long depolarisation steps were injected from a subthreshold potential to analyse spike frequency adaptation (SFA) and spike form. Potential post-inhibitory rebound-like properties were evoked by a protocol, rapidly hyperpolarising the cell from holding potential (-70 mV for uPNs and -60 mV for type I LNs) (Figure 5, D).

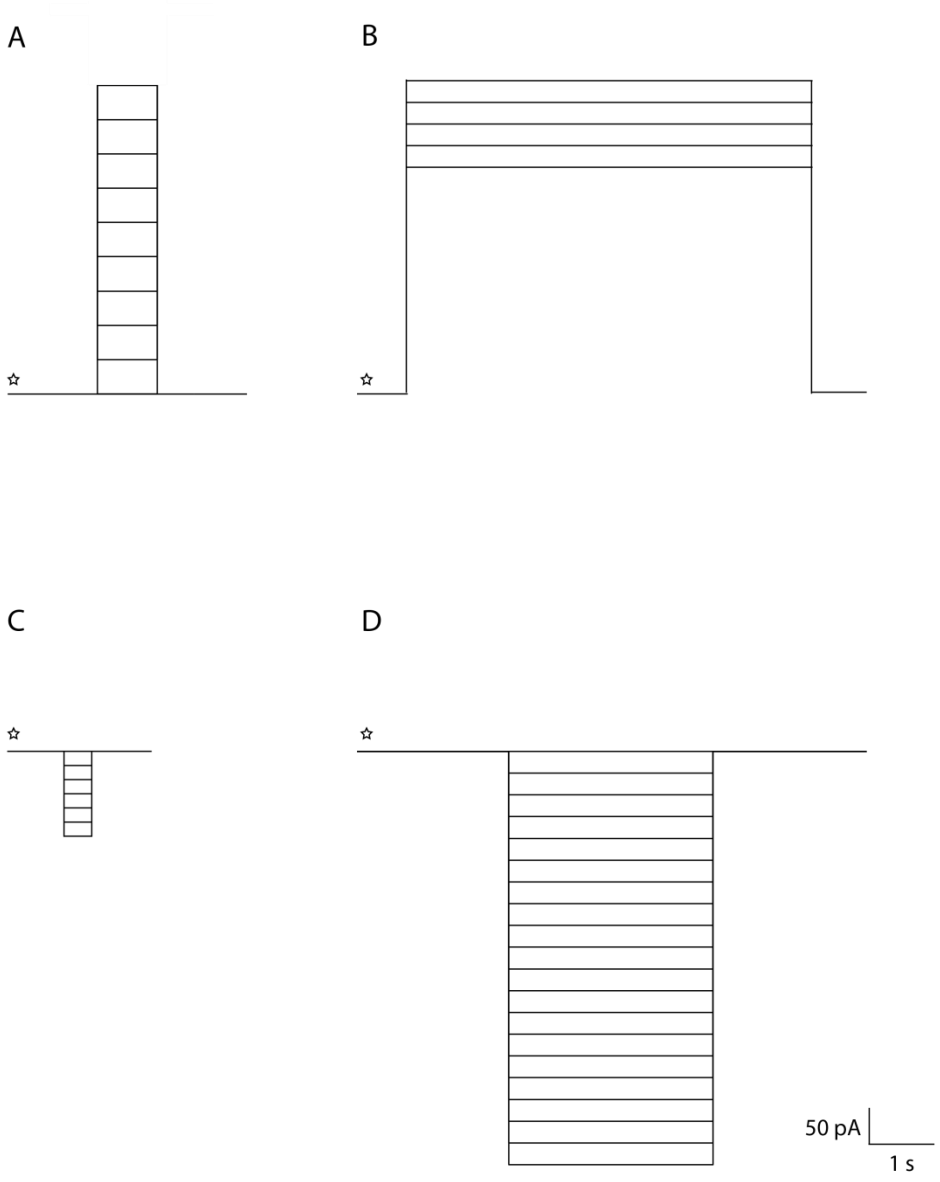

Figure 5: Current-clamp protocols for the characterisation of intrinsic firing properties of uPNs and type I LNs. (Description on following page)

(A) 1s lasting increasing (+50 pA) current steps were injected to determine spike threshold for each individual cell, from which in ***(B)*** the spike frequency adaptation over an incrementing (+5 pA or +30 pA) current steps was determined. Stimuli duration was set to 2.5 s or 6 s**.** ***(C)*** Input resistance (R_{inp}) was determined by hyperpolarisating current steps of -30 pA. ***(D)*** Post-inhibitory rebound protocol: decreasing current steps (-30 pA) were injected for 3 s followed by holding current. This protocol was also used to check for sag potentials. Asterisk indicates holding current.

3.2 Properties of type I LNs

Basic electrophysiological properties were analysed to define whether the type I LNs neuronal population in the antennal lobe of *Periplaneta americana* is a homogenous cluster with no variations in electrophysiological properties or rather a heterogeneous group with possible subpopulations. Type I LNs showed a mean resting potential of - 57.35 ± 6.13 mV (n = 12) and a mean cell capacitance of 32.60 ± 6.226 pF (n = 15).

3.2.1. Spike frequency adaptation

To investigate the spike frequency adaptation (SFA), a deceleration of spike frequency, long lasting depolarisating current steps were injected. All recorded type I LNs showed SFA. For a 2.5 seconds lasting stimuli two prominent neuron groups with different firing patterns were observed. *Strong adapting* (Figure 6, A1) neurons showed an initial high instantaneous frequency, which decreased within the first second to a steady state firing frequency (n = 13). In contrast, the second group of neurons showed *weak adaptation* (Figure 6, A2) in response to the same depolarisation with a frequency decrease of 1 Hz over the stimuli (n = 27).

Additionally, a third firing type was observed in response to a longer lasting depolarisation (6 s) referred to as *diphasic SFA* (Figure 6, B3). Neurons of this group (n = 10) reacted to injected depolarisations with a strong initial frequency decrease followed by a slow increase in frequency. The time dependency of the frequency modifications showed, that the phase of frequency acceleration could only be observed in response to stimuli longer than 2.5 seconds.

The specific frequency modifications were shown to be consistent over incrementing amplitude of current injection for *strong*- and *weak* adapting neurons (Figure 6, B1-2). However, in *diphasic* adapting type I LNs, the fast initial SFA was present only at higher mean instantaneous frequencies, while the frequency acceleration could be observed in all frequency ranges (Figure 6, B3).

The SFA in all three firing types of type I LNs was quantified as the instantaneous frequency ratio of the first AP doublet to the last AP doublet. (Figure 6, C). Classification of the SFA ratios was done according to ratio > 1.75 (mean) for strong adapting neurons and ratio < 1.75 for weak adapting neurons. In case of diphasic adapting neurons, the instantaneous frequencies over the whole stimulus were analysed.

Subthreshold depolarisating current injections revealed a depolarising hump directly after the stimulus onset (Figure 7) (n = 6). This hump exhibited an amplitude of approximately 1 mV and sustained for ~1 second. Afterwards, in response to the remaining stimuli duration, the membrane repolarised to a stabile potential.

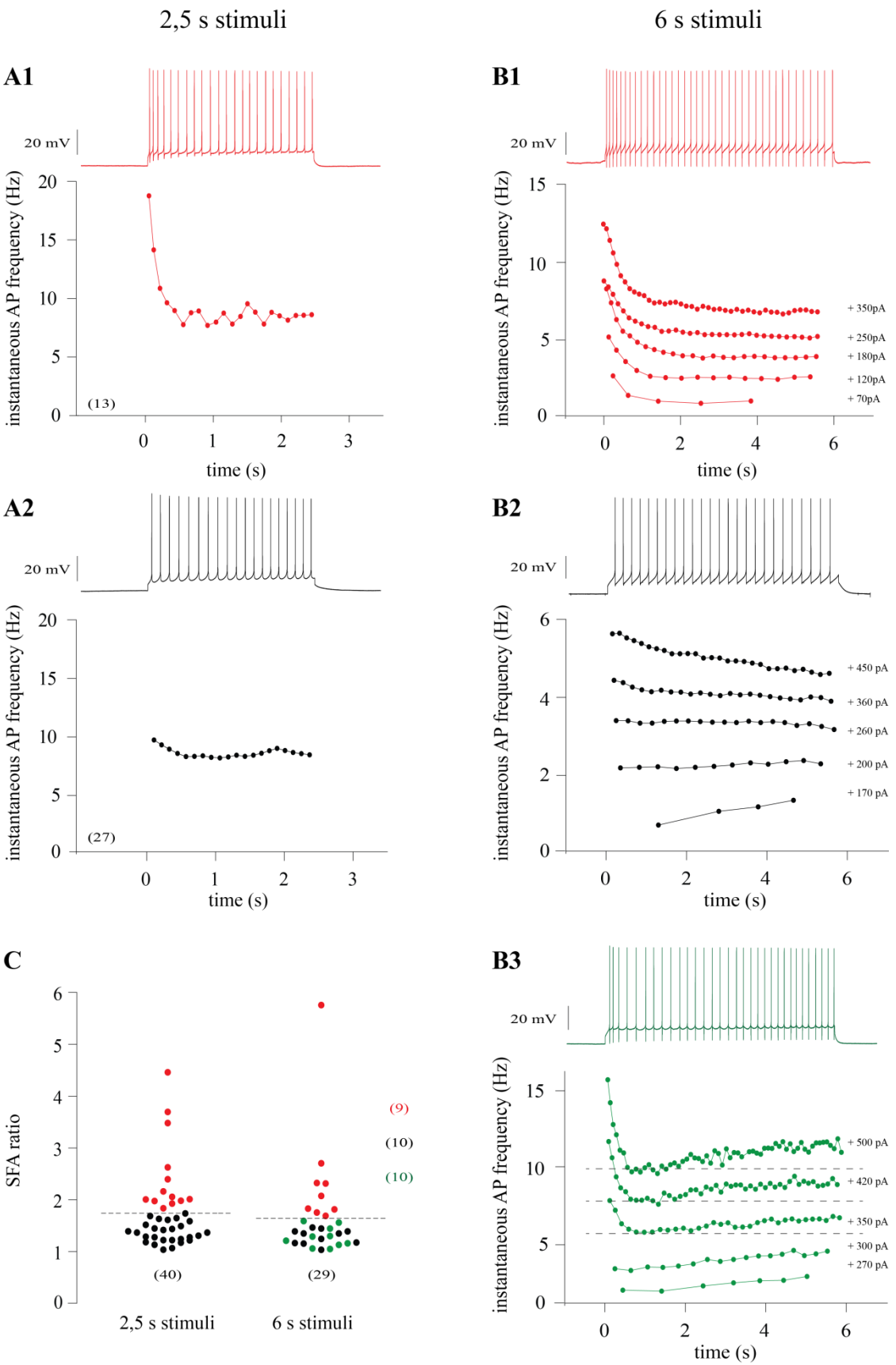

Figure 6: Spike frequency adaptation (SFA) patterns of type I LNs. (Description on following page)

(A1) *Strong SFA* (red) in response to a 2.5 s lasting stimulus. Spike train (upper panel) and corresponding instantaneous AP frequency curve (lower panel) plotted against the time. ***(A2)*** *Weak SFA* (black) in response to a 2.5 s lasting stimulus. Spike train (upper panel) and corresponding instantaneous AP frequency curve (lower panel) plotted against the time. ***(B1)*** *Strong SFA* (red) in response to a 6 s lasting stimulus. Representative spike train (upper panel) and corresponding instantaneous AP frequency curve (lower panel) for incrementing current injections plotted against the time. ***(B2)*** *Weak SFA* (black) in response to a 6 s lasting stimulus. Representative spike train (upper panel) and corresponding instantaneous AP frequency curve (lower panel) for incrementing current injections plotted against the time. ***(B3)*** *diphasic SFA* (green) in response to a 6 s lasting stimulus. Representative spike train (upper panel) and corresponding instantaneous AP frequency curve (lower panel) for incrementing current injections plotted against the time. Dashed lines mark the lowest instantaneous AP frequencies. ***(C)*** SFA ratios for 2.5 s and 6 s stimuli; colour code given as in ***A1*** and ***A2***, respectively ***B1***, ***B2*** and ***B3***. AP, action potential; SFA, spike frequency adaptation.

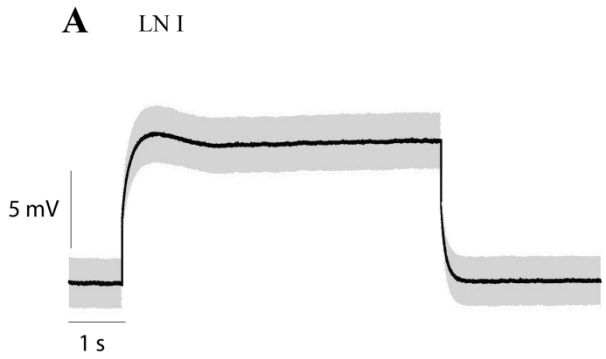

Figure 7: Type I LN subthreshold stimulation.

(A) Average (n = 6) of the responses to a subthreshold stimulation of type I LNs. Grey area indicates the SD of the average. SD, standard deviation.

3.2.2. Spike form

The spike form of each type I LN population was analysed based on the SFA classification (see 3.2.1).

The AP amplitude, width, maximal rate of repolarisation and the amplitude of the afterhyperpolarisation (AHP) showed no significant differences between *weak*-, *strong*- and *diphasic* adapting neurons (Figure 8, B1-4). However, the fast afterdepolarisation was shown to be significantly different between *weak*- and *strong* adapting neurons (*weak*: 2.646 ± 3.665 mV; *strong*: 6.643 ± 1.118 mV; p-value < 0,05), as well as between *weak*- and *diphasic* adapting neurons (*weak*: 2.646 ± 3.665 mV; *diphasic*: 3.880 ± 0.9755 mV; p-value < 0.05) (Figure 8, B5). In contrast the AP shape of neurons with *diphasic* SFA did not differ from that of the *strong* adapting neurons. Superimposed representative spikes of *strong* and *weak* adapting neurons are shown to demonstrate the difference in the fast after depolarisation (Figure 8, A1). The effect of this fast afterdepolarisation on an AP doublet is shown in Figure 8, A2. This effect repolarised the neuron within 1 ms, without affecting the amplitude of the previous hyperpolarisation, leading thereby to an increase in firing frequency. In contrast the slow repolarisation of the *weak* adapting neurons happens within a longer time.

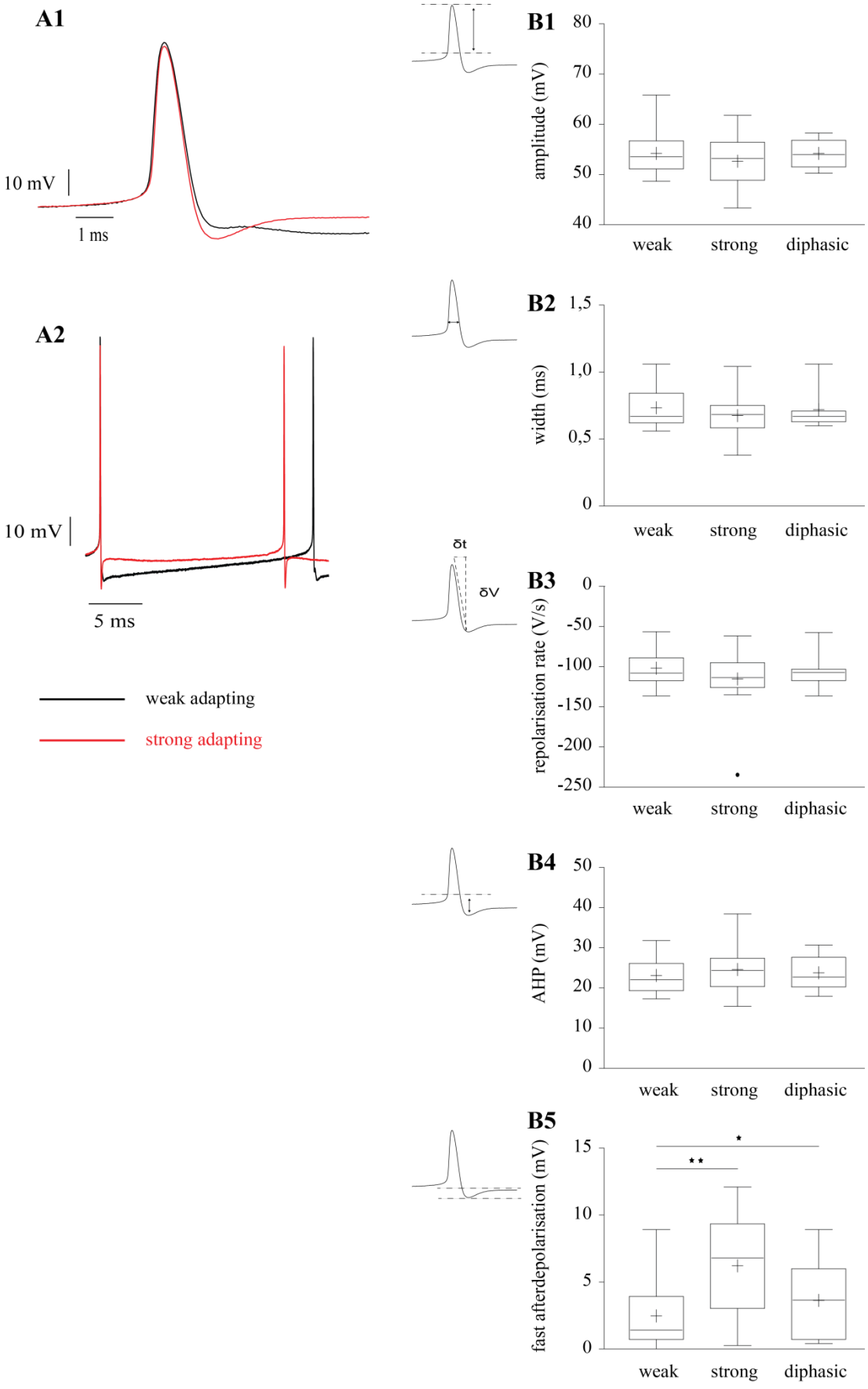

Figure 8: Action potential properties of *weak-* , *strong-* and *diphasic* adapting type I LNs. (Description on following page)

(A1) Spike overlay of representative first APs of a *weak* adapting (black) and a *strong* adapting (red) type I LNs. ***(A2)*** Representative example of an overlay of a spike train as an excerpt. *Weak* adapting (black), *strong* adapting (red). ***(B1-B5)*** Left: enlarged first AP, dashed lines and arrows indicate the measurements. ***(B1)*** Amplitude (mV) of AP was not altered between the different subpopulations. (weak: 55.15 ± 4.3 mV; strong: 53.49 ± 5.706 mV; diphasic: 55.16 ± 3.037 mV; p-value > 0.05). ***(B2)*** Spike width (ms) was not altered between the different subpopulations. (weak: 0.787 ± 0.16 ms; strong: 0.724 ± 0.16 ms; diphasic: 0.771 ± 0.15 ms; p-value > 0.05). ***(B3)*** Maximal rate of repolarisation (V/s) of AP was not altered between the different subpopulations. (weak: -91.57 ± 25.34 V/s; strong: -106.0 ± 44.80 V/s; diphasic: 93.51 ± 26.13 V/s; p-value > 0.05). ***(B4)*** AHP (mV) of AP was not altered between the different subpopulations. (weak: 24.81 ± 4.722 mV; strong: 26.41 ± 6.428 mV; diphasic: 25.51 ± 4.492 mV; p-value > 0.05). ***(B5)*** Fast afterdepolarisation (mV) of AP differed significantly between *weak*- and *strong* adapting neurons (weak: 2.646 ± 0.4948 mV; strong: 6.643 ± 1.118 mV; p-value < 0,05) and differed significantly between *weak*- and *diphasic* adapting neurons (weak: 2.646 ± 0.4948 mV; diphasic: 3.880 ± 0.9755 mV; p-value < 0.05). Values were statistically analysed using a one-way-ANOVA (p = 0.05; p-value: ns > 0.05) and are given as mean ± SD . AP, action potential; AHP, afterhyperpolarisation; SD, standard deviation.

In addition to the analysed differences in AP forms of the three type I LN subpopulations, their input resistances were compared. Here, values were not significantly different, so that the mean input resistance for type I LNs can be considered as 30.74 ± 8.221 mV (Figure 9) (n = 38).

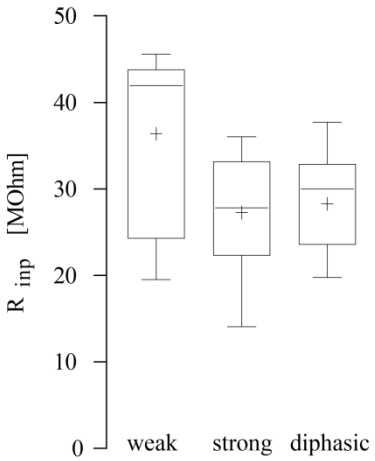

R_{inp} [MOhm]

n	weak	strong	diphasic	(38)
mean	35.83	26.78	27.81	30.74
SD	10.43	7.034	5.772	8.221
SEM	3.475	2.345	1.740	1.334

Figure 9: Input resistance for *weak*-, *strong*- and *diphasic* adapting neurons.
Boxplots (left) with respective data table (right) of R_{inp}–analysis. Values are giving as the means ± standard deviation (SD) and standart error of the mean **(**SEM**)** in MOhm. R_{inp}, input resistance.

3.2.3. Post-inhibtory rebound friring and sag potential in type I LNs

For the following experiments, when hyperpolarising currents were injected, the cells were pooled.

In response to hyperpolarizing current injections, post-inhibtory rebound firing could be observed at the offset current step (Figure 10, A1). Descending current steps were injected and the mean membrane potential of hyperpolarising prepulse nessesary to elicit the first post-inhibitory firing was -88,489 ± 8,451 mV (n = 17) (Figure 10, A2). When further hyperpolarising the cells to membrane potentials to -116,024 ± 19,451 mV (n = 11), a sag potential could be observed (Figure 10, B1-2).

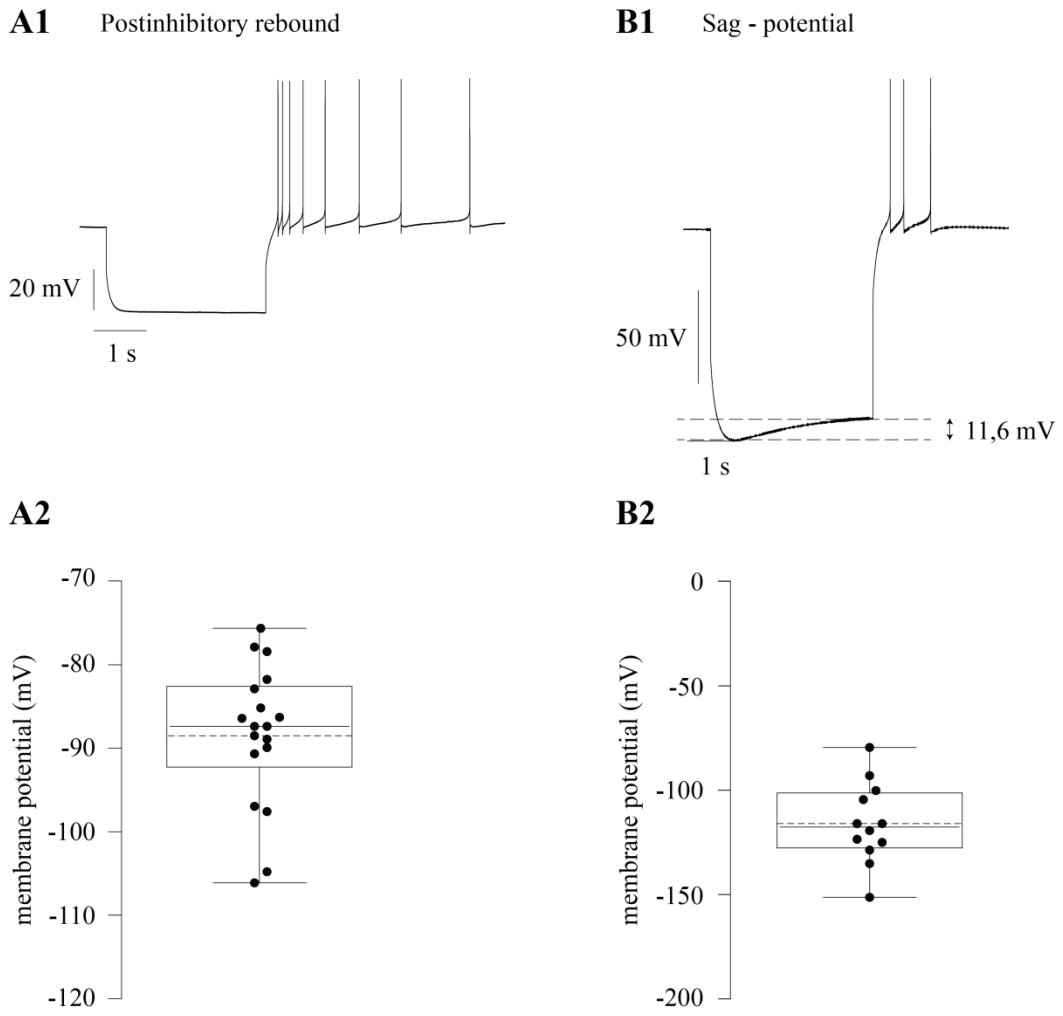

Figure 10: Postinhibitory rebound and sag potential of type I LN (Description on following page).

(*A1)* Hyperpolarising current injections evoked postinhibitory rebound firing at the offset current injection. ***(A2)*** Membrane potential of the hyperpolarising prepulse that elicited the first postinhibitory rebound AP. Mean value as dashed line, -88.489 ± 8.451 mV (n = 17). ***(B1)*** Stronger hyperpolarisations elicited a sag potential. ***(B2)*** Membrane potential when first sag potential could be observed. Mean value given as dashed line, -116.024 ± 19.451 mV (n = 11).

3.3 Properties of uPNs

Basic electrophysiological properties were analysed to define whether the uPNs neuronal population in the antennal lobe of *Periplaneta americana* is a homogenous cluster with no variations in electrophysiological properties or rather a heterogeneous group with possible subpopulations. uPNs showed a mean resting potential of - 57.35 ± 6.13 mV (n = 12) and a mean cell capacitance of 32.60 ± 6.226 pF (n = 15). The recorded uPNs mean input resistance was 49.12 ± 15.28 MΩ.

3.3.1. Spike frequency acceleration in uPNs

To investigate the spike frequency modulation, long lasting depolarising currents were injected. All recorded uPNs showed an acceleration in their AP frequency in response to a sustained depolarisating stimulus. The SFA in uPNs was quantified using the instantaneous frequency ratio (SFA ratio) of the first AP doublet to the last AP doublet (Figure 11, B). All tested uPNs showed a SFA ratio < 1. Frequency acceleration was shown to be consisting over incrementing amplitudes of current injection (Figure 11, A), but especially strong when high mean frequencies were evoked. Furthermore acceleration was observed to continue over the whole stimulus.

When cells were stimulated with subthreshold depolarising current injections, a depolarising voltage ramp over the stimulus could be observed (Figure 12) (n= 6). This lead to a depolarisation of approximately 2.5 mV at stimulus offset in comparison to stimulus onset.

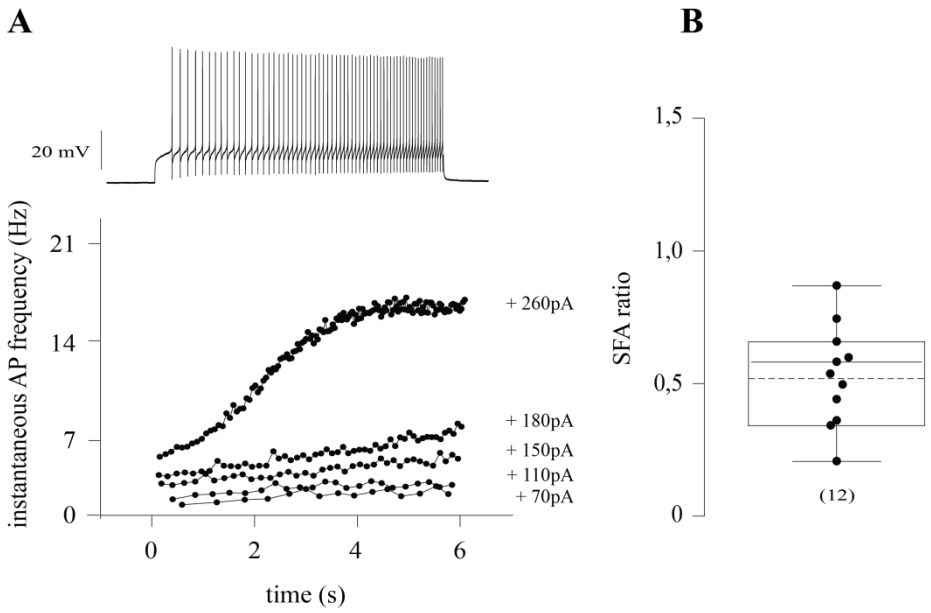

Figure 11: Spike frequency modulation of uPNs.

(A) Representative Spike train (upper panel) and corresponding instantaneous AP frequency (lower panel) for incrementing current injections plotted against the time. ***(B)*** SFA ratios for 6 s stimuli (n = 11). AP; action potential, SFA, spike frequency adaptation.

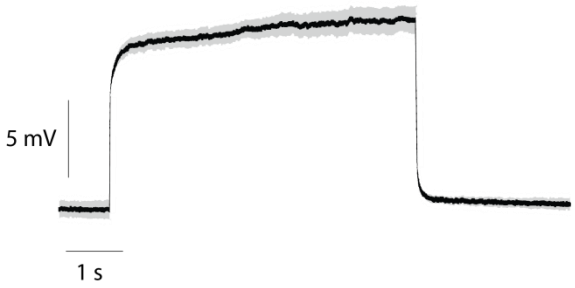

Figure 12: uPN subthreshold stimulation

(A) Average (n = 6) of the responses to a subthreshold stimulation of uPNs. Grey area indicates the SD of the average. SD, standard deviation.

3.3.2. Spontaneous burst-like firing of uPNs

6 out of 18 recorded uPNs showed a spontaneous, burst like firing when no current was injected. The cells fired an approximately 5.5 ± 0.36 s lasting burst. The duration between two bursts lasted 8.7 ± 1.5 s.

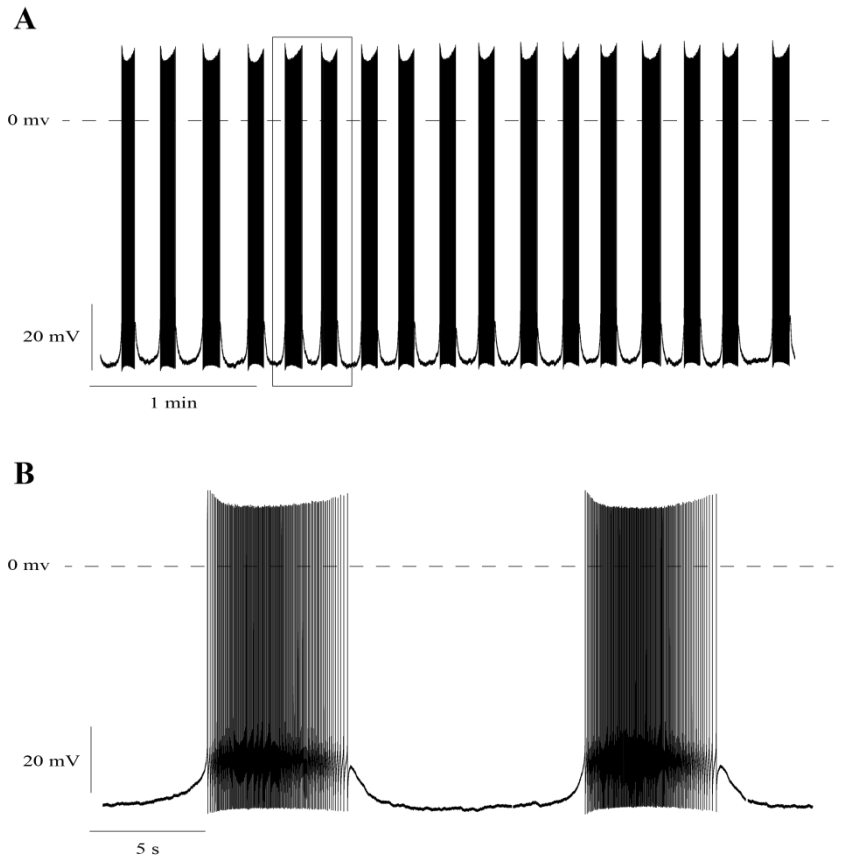

Figure 13: Spontaneous burst-like firing of uPNs.
33% (n = 6) of tested neurons showed a spontaneous burst-like firing when 0 pA were injected. Duration of bursts: 5.5 ± 0.36 s, duration between bursts: 8.7 ± 1.5 s.

3.3.3. Spike form of uPNs

In a next step, the spike form of the uPNs was analysed. The results are graphically shown in Figure 14. The average amplitude of APs was 45.53 ± 8.935 mV. Spike width was measured as 0.442 ± 0.114 ms. The mean maximal rate of repolarisation was -175.1 ± 41.53 V/s and the AHP 37.81 ± 6.991 mV. Values are given as mean ± SD.

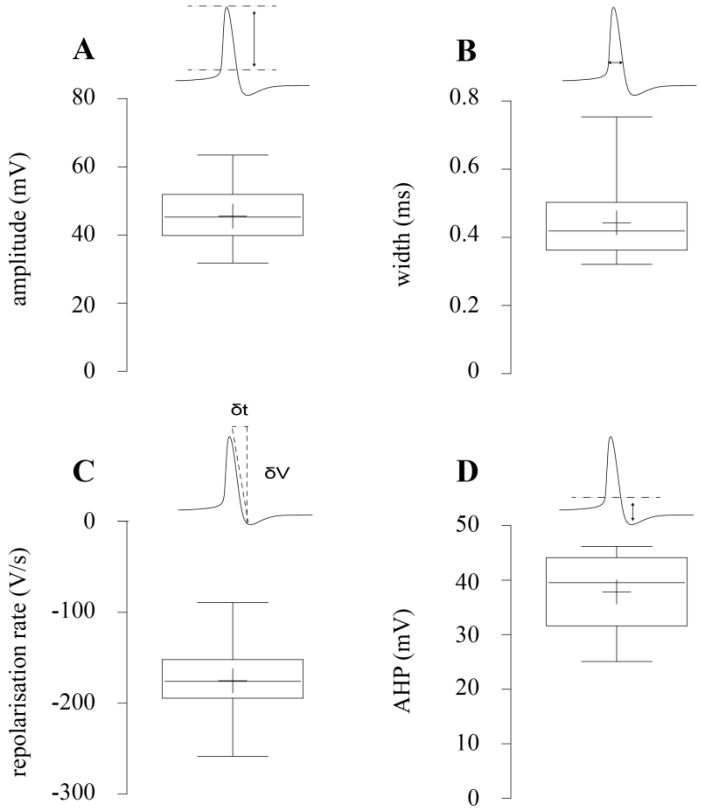

Figure 14: Spike form of uPNs. ***(A-D)*** upper panel enlarged first AP, dashed lines and arrows indicate the measurements. ***(A)*** Amplitude of AP: 45.53 ± 8.935 mV. ***(B)*** Spike width: 0.442 ± 0.114 ms. ***(C)*** Maximal rate of repolarisation (V/S): -175.1 ± 41.53 V/s. ***(D)*** AHP (mV) of AP: 37.81 ± 6.991 mV. Values are given as mean ± SD. AP, action potential; AHP, afterhyperpolarisation.

3.3.4. Post-inhibtory rebound potentials and sag potential of uPNs

uPNs showed no postinhibitory firing in response to hyperpolarising current injections (Figure 15, A). When hyperpolarising the cells to membrane potentials of -88.779 ± 9.972 mV (n = 8) a sag potential could be observed (Figure 15, B1-2).

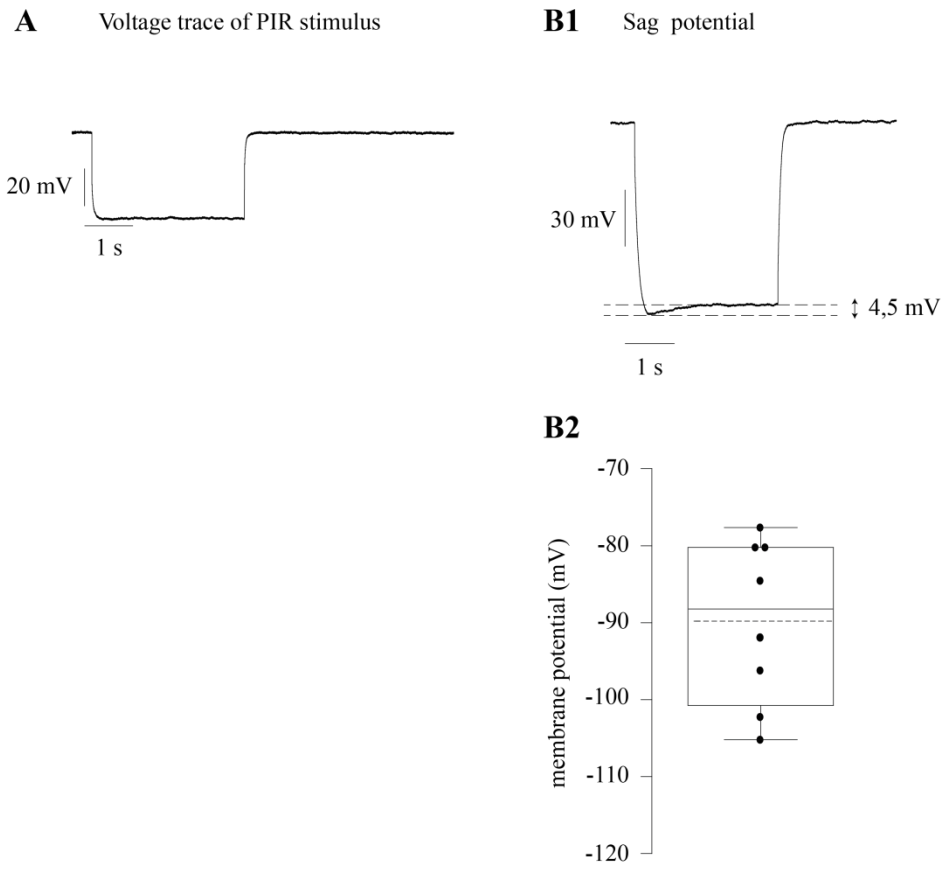

Figure 15: Voltage trace of PIR and the sag-potential of uPNs.

(*A)* Hyperpolarising current injection did not evoke any postinhibitory rebound like properties in uPNs. ***(B1)*** Stronger hyperpolarisations elicited a sag potential. ***(B2)*** Membrane potential when the first sag potential could be observed. Mean value as dashed line, -88.779 ± 9.972 mV (n = 8). Cells were held at -70 mV. PIR: post inhibitory rebound.

3.4 Comparison between type I LNs and uPNs

Comparing the two populations of antennal lobe neurons type I LNs and uPNs, they showed major differences in the response to depolarising stimuli. Subthreshold current injection elicited a depolarised voltage hump in type I LNs, while same injections produced depolarising voltage ramps in uPNs (Figure 16, A,B and Figure 17). A possible connection between the mentioned subthreshold voltage hump for type I LNs and

Subrathreshold current injections caused adapting spike trains of type I LNs, uPNs showed an acceleration in instantaneous AP frequency. While type I LNs showed three different adaptation patterns (Figure 16, C1-3), all uPNs showed frequency acceleration and were further considered as a homogenous neuron population.

Comparing the spike form between uPNs and the three type I LNs subtypes, all criteria show significant differences.
The threshold (mV) of APs showed significant differences between uPNs and diphasic adapting type I LNs (uPN: -27.95 ± 3.153 mV; diphasic: -31.69 ± 3.254 mV; p-value < 0.05) and uPNs and strong adapting LNI (uPN: -27.95 ± 3.153 mV; strong: -34.61 ± 3.425 mV; p-value < 0.05), but showed no significant differences to weak adapting type I LNs (weak: -30.36 ± 4.279 mV). The amplitude (mV) of APs was significantly decreased in uPNs compared to all three groups of type I LNs (uPN: 45.53 ± 8.935 mV; diphasic: 55.16 ± 3.037 mV; strong: 53.49 ± 5.706 mV; weak: 55.15 ± 4.300 mV; p-values < 0.05). The spike width (ms) of uPNs was significantly reducedin comparison to type I LNs (uPN: 0.442 ± 0.11 ms; diphasic: 0.771 ± 0.15 ms; strong: 0.724 ± 0. 16 ms; weak: 0.787 ± 0.16 ms; p-values < 0.05). Also the maximum rate of repolarisation (V/s) was significantly increased in uPNs (uPN: -175.1 ± 41.53 V/s; diphasic: -93.51 ± 26.13 V/s; strong: -106 ± 44.8 V/s; weak: -91.57 ± 25.34 ms; p values < 0.05). The AHP (mV) of uPNs showed a significant increase compared to the three groups of type I LNs (uPN: 37.81 ± 6.991 mV; diphasic: 25.51 ± 4.492 mV; strong: 26.41 ± 6.428 mV; weak: 24.81 ± 4.722 ms; p-values < 0.05) (see also Figure 18, Appendix).

In contrast to uPNs (Figure 15, A), type I LNs generated APs in response to hyperpolarising current injections (Figure 10, A), referred to as post inhibitory rebound.

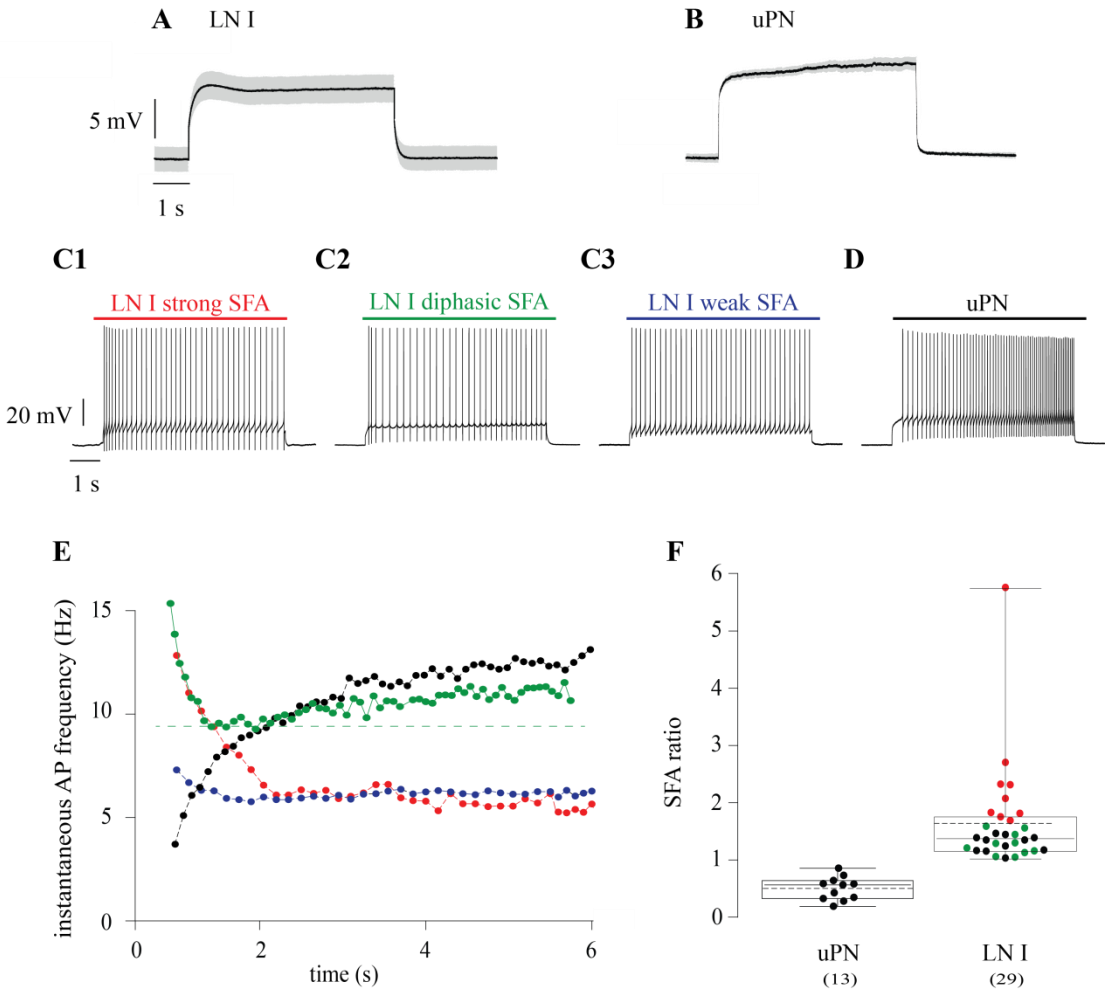

Figure 16: Comparison of type I LNs and uPNs.

(A) subthreshold stimulation of a LN I produces a characteristic voltage hump at the onset of stimulus, lasting for ~1 s. Afterwards neuron repolarised to steady state potential. Average curve (n = 6), grey area indicates SD of average. ***(B)*** subthreshold stimulation of a uPNs produces a characteristic voltage ramp over the whole stimulus. Average curve (n = 6), grey area indicates SD of average. ***(C1-D)*** Representative spike trains in response to 6 s lasting current injections. ***(E)*** Characteristic instantaneous AP frequencies plotted against the time of stimulus. Single experiments, representing the different cell types shown in ***(C1-D)***. Colourcode correspond to given cell types. ***(F)*** SFA ratios calculated as the fraction of the initial instantaneous frequency and the final instantaneous frequency for 6 s depolarisations. SFA ratios for LN I (n = 29) and uPNs (n = 13), colourcode given in ***(C1-D)***. AP, action potential; SFA, spike frequency adaptation.

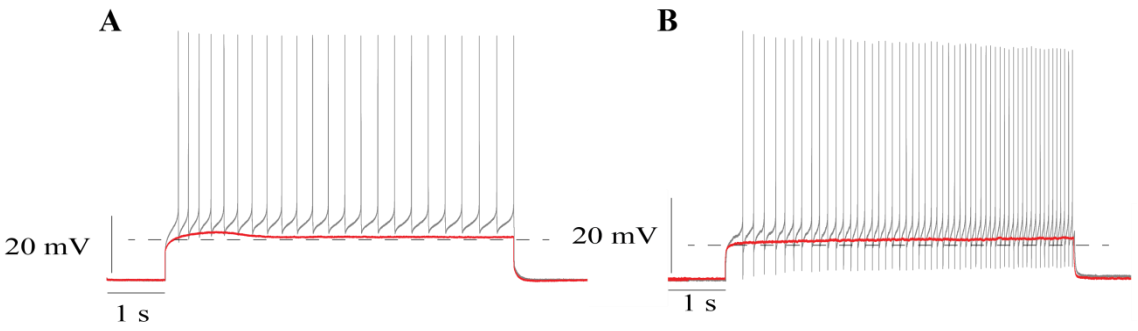

Figure 17: Subthreshold stimulation evoked a characteristic depolaraisation. ***(A)*** Subthreshold stimulations of type I LNs caused a depolarising voltage hump (red). AP firing (grey) caused by a higher depolarisations showed high frequencies temporally correlating to the hump. ***(B)*** Subthreshold stimulations of uPNs caused a depolarising voltage ramp (red). AP firing (grey) caused by a higher depolarisations showed a frequency acceleration temporally correlating to voltage ramp. Dashed lines serve as an orientation for the voltage changes.

4 | Discussion

The aim of this bachelor thesis was to characterise the intrinsic firing properties of type I LNs and uPNs in the AL of the cockroach *Periplaneta Americana.*

4.1. Spike frequency modulation

In order to study the cell intrinsic spike frequency modulations, long lasting depolarisating currents were injected. The responses of type I LNs and uPNs were either tested to 2.5 s and 6 s lasting stimuli. The results of the experiments showed, that type I LNs and uPNs showed different spike frequency adaptation- and modulation patterns.

4.1.1 Spike frequency adaptation in type I LNs

Previous studies revealed that type I LNs exhibit GABA-like immunoreactivity and are able to generate Na^+-driven action potentials in response to odour stimulation and depolarisating current injections (Husch et al. 2009). Furthermore the type I LN neuron population has been regarded as a homogenous population (Husch et al. 2009 a). In this thesis it could be shown that all type I LNs show SFA in response to depolarisating stimuli, however the frequency modulation is not homogenous: in response to 2.5 s lasting stimuli injections, two adaptation patterns were observed: strong adapting type I LNs showed a high frequency at the onset of stimulus and the frequency decreased by 50% over the remaining stimulus. Weak adapting type I LNs showed also SFA, but in contrast the frequency dropped less than 50%. When depolarisating stimulus was expanded to 6 s, both populations were consistent, but a third population of diphasic adapting neurons became apparent. Here a strong SFA at the onset of stimulus was followed by a frequency accelerated after ~2 s. In all three different subpopulations, SFA happened within the first second of stimulus. Remarkably, it was observed that a subthreshold stimulation of type I LNs evoked a depolarising voltage hump at the onset of stimulus, persisting for ~1 s. The general mechanism of SFA is closely related to the

opening of voltage gated Ca^{2+} channels during the depolarising phase of an AP and subsequent activations of Ca^{2+} activated K^{+} channels, which are responsible for the lowering of membrane potential and thereby lowering the AP frequency (Sah & Davies 2000). However former studies showed that blocking the BK_{Ca}-channels of type I LNs did not result in a loss of SFA (Bachelor-thesis, Sandra Wendler 2012). Additionally, recent experiments point towards the fact that type I LNs does not have SK_{Ca}-channels (personal communication with Viktor Bardos). Together, these results point in the direction of another underling mechanism responsible for SFA in type I LNs. The fact that the subthreshold evoked voltage hump temporarily correlates with the phase of highest frequency (Figure 17, A), suggests that this mechanism might contribute to the SFA. Higher depolarising voltages at the onset of stimulus, evoked by the hump, could result in higher AP frequencies, which decelerate due to the repolarisation to a steady potential after the hump. It was observed, that the AP frequency reached a steady state after the adaptation in weak- and strong adapting type I LNs. In the third population of diphasic adapting type I LNs the acceleration of frequency is probably caused by an additional mechanism that might be similar in uPNs.

4.1.2 Spike frequency acceleration in uPNs

uPNs showed an acceleration in their AP frequency in response to the depolarising stimuli. It was shown, that this effect is consistent for different stimulus current amplitudes as well as for different stimuli durations. The mechanism contributing to this reverse adaptation patterns might be related to a combination of high-voltage activated Ca^{2+} currents and persistent Na^{+} currents that open during AP firing and this effect increases over a long spike train (Wilson et al. 2004). However also for uPNs, a subthreshold stimulation revealed a possible mechanism contributing in frequency acceleration (Figure 17, B): low current injections that did not evoke APs during a stimulus resulted in a depolarising voltage ramp. Here, the frequency acceleration seems to be a result of the higher voltages of this ramp. This suggests that the mechanism underlying acceleration does not require spiking. This voltage ramp could either be caused by a slow activation of inward ion currents or a slow inactivation of outward ion currents. Frequency acceleration in layer 5 pyramidal neurons of mice was already demonstrated to be DTX Dentrotoxine (DTX) sensitive (Miller et al. 2008). DTX is

known to block voltage gated potassium channels that conduct the transient potassium current (I_A). Therefore the steady depolarisation observed in uPNs might be linked to the steady inactivation of the I_A, resulting in a slow inactivation of K^+ outward currents.

4.1.3 The role of spike frequency modulation in the olfactory network

Different types of SFA point towards differences in expression of types and number of ion channels, which was already been shown for vertebrates and invertebrates (Powers et al. 1999; Stocker 2004). The modulation of spike frequency, e.g. SFA, in neuronal circuits is considered to be a modulating mechanism that reduces excitability in response to a sustained stimulus. Therefore the SFA can be seen as a source for neuronal plasticity. For the locusts lobula giant movement detector (LGMD), a visual interneuron that exhibits rapid adaptation to both current injection and visual stimuli, it was observed that the interneuron showed high frequency at stimulus onset but SFA and reduced excitability to a sustained stimulus (Peron & Gabbiani 2009). Here, SFA was interpreted to serve as a ”selectivity filter for specific temporal input profiles”. A similar role is conceivable in the cockroaches AL for the *strong* adapting type I LNs which are supposed to shape the tuning profiles of the uPNs within the olfactory network. Another study in the crickets auditory system showed, that SFA can be seen as “forward masking” (Sobel & Tank 1994; Liu & Wang 2001), where interneurons effectively select the strongest input among competing sources of input signals. Both examples for SFA in interneurons of insect sensory systems suggesst, that this phenomenon serves as a filtering system for olfactory information. Therefore different SFA patterns within the heterogenic group of type I LNs might be useful to sharpen the responses to different olfactory stimuli *in vivo* and thus to help discriminate different odours.

The observed frequency acceleration of uPNs might be crucially involved in circuit dynamics as it probably serves as a cellular amplifier and increases correlations and signals among syntactical coupled neuron populations. Since the results revealed an AP frequency acceleration over a long lasting stimulus, it seems like the duration of a stimulus is frequency coded. A similar mechanism might be the case for *diphasic* adapting type I LNs which might amplify a signal in regard to the length of stimulation.

4.2. Rebound and sag potential

The results of this thesis show, that type I LNs in contrast to the tested uPNs showed postinhibitory rebound firing. A postinhibitory rebound (PIR) is defined as a "membrane depolarisation at the offset of a hyperpolarising stimulus" (Angstadt et al. 2005). The currents generating and shaping the PIR properties are complex and multifactorial: Hyperpolarisations can lead to a deinactivation of subthreshold Ca^{2+} currents which then subsequently activate and lead to a transient depolarisation. Another mechanism is the activation of the hyperpolarisation-activated current (I_h/I_f), producing a depolarising sag potential. Furthermore, voltage dependent Na^+ channels become deinaktivated due to hyperpolarisation. At the offset of the hyperpolarising stimulus, the high number of available Na^+ currents together with Ca^{2+} currents lead to an influx of positive ions and therefore to a suprathreshold potential and AP firing.

Regarding the fact, that no PIR was observed for uPNs possible reasons might be a probably different channel composition in these neurons compared to type I LNs. The I_A, a transient K^+ current, can act as an antagonist to the spontaneous opening of deinactivated Na^+ channels: When cells are released from the inhibition, these Na^+ channels open spontaneously resulting in a Na^+ influx and a further depolarisation of the membrane. However, the hyperpolarisation also deinactivates the I_A channels which then can activate at the offset of inhibition resulting in a K^+ efflux that prevents the membrane from a Na^+ driven depolarisation. As described, uPNs are known to have a higher I_A current-density then type I LNs (diploma thesis, Lars Paeger 2008) suggesting that here more K^+ ions leave the cell via I_A channels and therefore hyperpolarise the membrane.

When strong hyperpolarising currents were injected, both, type I LNs and uPNs showed a depolarising current, the sag potential. This depolarisation is caused by the I_h current conducted by hyperpolarisation-activated cyclic nucleotide-gated channels (HCN). Structurally, these channels belong to the superfamily of voltage-gated K^+ (Kv) channels. Although HCN channels are permeable for K^+- and Na^+ ions they conduct Na^+ under strongly hyperpolarised conditions, due to the higher driving force for Na^+ than for K^+.

4.4 Input resistance Type I LNs and uPNs

Since the cell membrane can be described as an electrical RC-circuit, the determination of the input resistance (R_{inp}) follows Ohm´s law. The input resistance of the three subpopulations of type I LNs were compared. Here, no significant difference could be observed. Since the different adaptation behaviours are thought to be related to different current compositions, the R_{inp} revealed no significant differences in all-currents density. In comparison to the uPNs R_{inp} a strong difference becomes obvious. As mentioned above, the current density for different current compositions seems to be different

4.5 Spontaneous burst-like firing of uPNs

33% of all recorded uPNs showed a burst-like firing when no current was injected (Figure 13). As mentioned, uPNs receive GABAergic input from type I LNs in the antennal lobe. For the shown experiments, all GABAergic synaptical transductions were blocked. $GABA_A$ and $GABA_B$ was blocked by Picrotoxin (PTX) and CGP, respectively. The results suggest, that the permanent block of this inhibitory neurotransmitter results in a disinhibition of uPNs. The resulting burst-like firing therefore might be intrinsic. The regularity of the event could support this thesis. However, although all known excitatory inputs were blocked, other neurotransmitters, for example octopamine, might have an excitatory effect. Furthermore, spontaneous burst-like activity was already shown for neurons from the posterodorsal deutocerebrum which also innervate glomeruli of the AL (Fusca, 2012.Inaugural-Dissertation). Here it might be possible, that uPNs burst-like firing is related to a not complete block of synaptic transmission. Generally, the results suggest, that uPNs receive permanently inhibitory input from type I LNs and therefore leading to a downregulation of excitability.

4.5 Outlook

The results of this thesis demonstrate that the neuron population of type I LNs consists of at least three different types of neurons. These subpopulations differ in their specific SFA pattern. Since no distinct differences in the specific innervation patterns could be observed, further investigation might reveal specific differences. Especially *diphasic* adapting type I LNs should be further characterised:

Since subthreshold stimuli revealed characterising voltage modulations, which fitted to the spike frequency modualtions, it would be interesting to investigate the underling mechanisms. In further approaches Tetrodotoxin (TTX) and Cadmium (Cd) could be applied to block voltage-activated Na^+ currents and Ca^{2+} currents respectively. By blocking voltage-activated Na^+ currents, both the observed depolarising voltage humps and the ramp could be further characterised, since no Na^+ driven APs would be generated. The application of TTX and Cd could also reveal, if Na^+ currents, Ca^{2+} currents or both of them are responsible for the depolarisation. In addition to these investigations, the impact of the I_A on spike frequency acceleration of uPNs and *diphasic* adapting type I LNs should be investigated. Since spike frequency acceleration in neocortical interneurons in mice was found to be DTX sensitive (Miller et al. 2008), a specific I_A current blocker, DTX could be applied during recordings of *diphasic* adapting type I LNs and uPNs, as well. Spike frequency acceleration of uPNs might encode both, the olfactory stimuli intensity and the duration of the stimulus. Long lasting odour stimulation experiments could support this theory in future experiments.

5 | Appendix

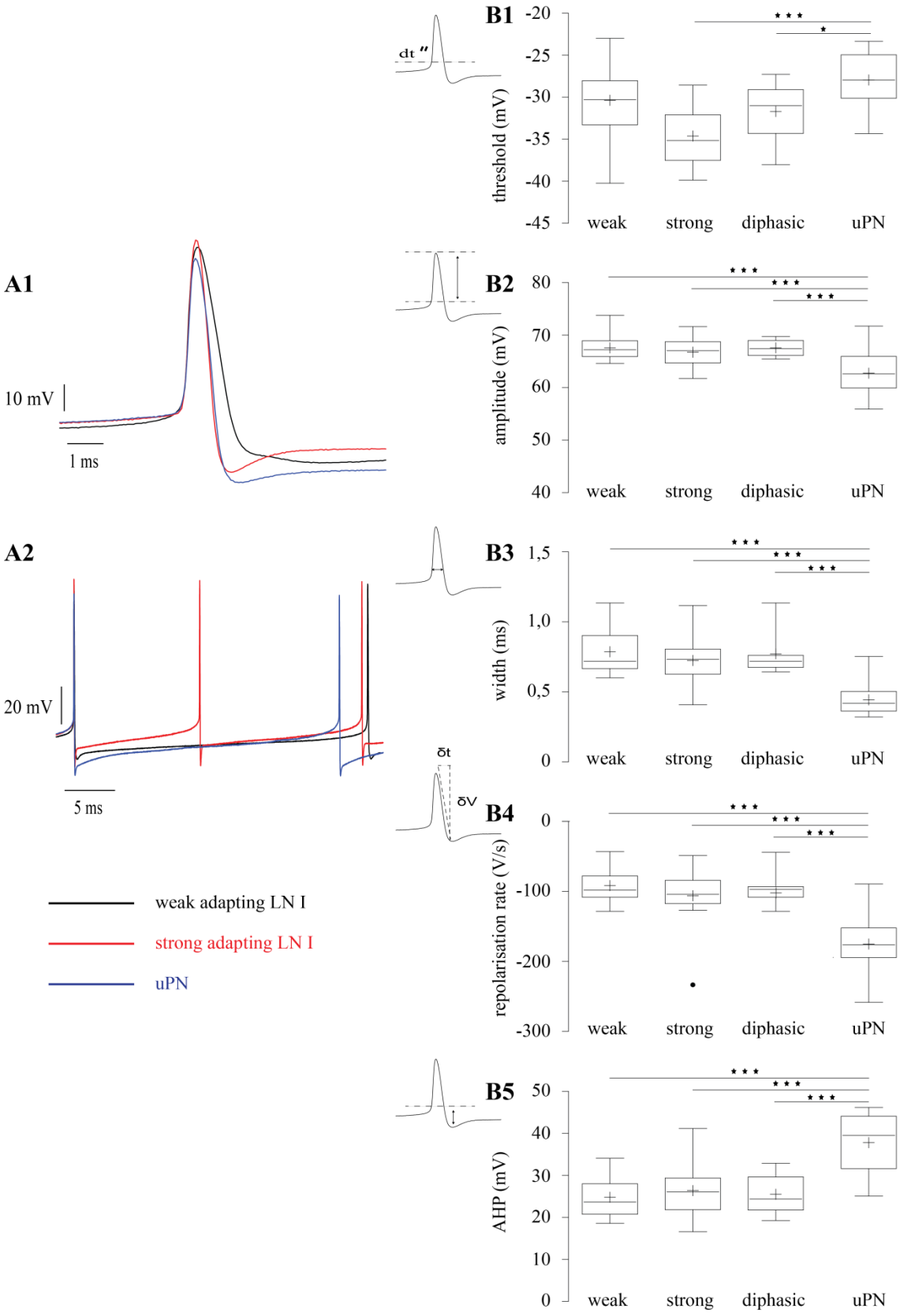

Figure 18: Action potential properties type I LNs and uPNs. (Description on following page.)

(A1) Representative example a spike overlay of the first AP for weak- (black), strong adapting (red) type I LNs and an uPNs (blue). ***(A2)*** Representative example of an overlay of spike trains as an excerpt, colourcode given in ***(A1).*** ***(B1-B5)*** Left: enlarged first AP; dashed lines and arrows indicate the measurements. ***(B1)*** Threshold (mV) of AP showed significant differences between uPNs and diphasic adapting LNI (uPN: -27.95 ± 3.153 mV; diphasic: -31.69 ± 3.254 mV; p-value < 0.05) and uPNs and strong adapting LNI (uPN: -27.95 ± 3.153 mV; strong: -34.61 ± 3.425 mV; p-value < 0.05), but showed no significant differences to weak adapting LN I (weak: -30.36 ± 4.279 mV). ***(B2)*** Amplitude (mV) of AP was significantly different between all three groups of LNIs in comparison to uPNs (uPN: 45.53 ± 8.935 mV; diphasic: 55.16 ± 3.037 mV; strong: 53.49 ± 5.706 mV; weak: 55.15 ± 4.300 mV; p-values < 0.05). ***(B3)*** Spike width (ms) was significantly different between all three groups of LNIs in comparison to uPNs (uPN: 0.442 ± 0.11 ms; diphasic: 0.771 ± 0.15 ms; strong: 0.724 ± 0. 16 ms; weak: 0.787 ± 0.16 ms; p-values < 0.05). ***(B4)*** Maximal rate of repolarisation (V/s) was significantly different between all three groups of LNIs in comparison to uPNs (uPN: -175.1 ± 41.53 V/s; diphasic: -93.51 ± 26.13 V/s; strong: -106 ± 44.8 V/s; weak: -91.57 ± 25.34 ms; p-values < 0.05). ***(B5)*** AHP (mV) was significantly different between all three groups of LNIs in comparison to uPNs (uPN: 37.81 ± 6.991 mV; diphasic: 25.51 ± 4.492 mV; strong: 26.41 ± 6.428 mV; weak: 24.81 ± 4.722 ms; p-values < 0.05). Values were statistically analysed using a one-way-ANOVA (p = 0.05; p-value: ns > 0.05). AP, action potential; AHP, afterhyerpolarisation.

List of figures

References

Angstadt, J.D. et al., 2005. Mechanisms of postinhibitory rebound and its modulation by serotonin in excitatory swim motor neurons of the medicinal leech. *Journal of comparative physiology. A, Neuroethology, sensory, neural, and behavioral physiology*, 191(8), pp.715–32. Available at: http://www.ncbi.nlm.nih.gov/pubmed/15838650 [Accessed September 27, 2014].

Boeckh, J. & Ernst, K.-D., 1987. Contribution of single unit analysis in insects to an understanding of olfactory function. *Journal of Comparative Physiology A*, 161(4), pp.549–565. Available at: http://link.springer.com/10.1007/BF00603661 [Accessed September 27, 2014].

Christensen, T.A. et al., 1993. Local interneurons and information processing in the olfactory glomeruli of the moth Manduca sexta. *Journal of comparative physiology. A, Sensory, neural, and behavioral physiology*, 173(4), pp.385–99. Available at: http://www.ncbi.nlm.nih.gov/pubmed/8254565 [Accessed September 29, 2014].

Davis, R.L., 2004. Olfactory learning. *Neuron*, 44(1), pp.31–48. Available at: http://www.sciencedirect.com/science/article/pii/S089662730400577X [Accessed September 12, 2014].

Ernst, K.D., Boeckh, J. & Boeckh, V., 1977. A neuroanatomical study on the organization of the central antennal pathways in insects. *Cell and Tissue Research*, 176(3). Available at: http://link.springer.com/10.1007/BF00221789 [Accessed September 28, 2014].

Hamill, O.P. et al., 1981. Pfltigers Archiv Improved Patch-Clamp Techniques for High-Resolution Current Recording from Cells and Cell-Free Membrane Patches. , pp.85–100.

Hildebrand, J.G. & Shepherd, G.M., 1997. Mechanisms of olfactory discrimination: converging evidence for common principles across phyla. *Annual review of neuroscience*, 20, pp.595–631. Available at: http://www.ncbi.nlm.nih.gov/pubmed/9056726 [Accessed September 11, 2014].

Husch, A. et al., 2009. Calcium current diversity in physiologically different local interneuron types of the antennal lobe. *The Journal of neuroscience : the official journal of the Society for Neuroscience*, 29(3), pp.716–26. Available at: http://www.ncbi.nlm.nih.gov/pubmed/19158298 [Accessed September 27, 2014].

Husch, A. et al., 2009a. Distinct Electrophysiological Properties in Subtypes of Nonspiking Olfactory Local Interneurons Correlate With Their Cell Type-Specific Ca2+ Current Profiles. *Journal of Neurophysiology*, 102(5), pp.2834–2845. Available at: http://www.ncbi.nlm.nih.gov/pubmed/19759323 [Accessed September 2, 2014].

Husch, A. et al., 2009b. Distinct Electrophysiological Properties in Subtypes of Nonspiking Olfactory Local Interneurons Correlate With Their Cell Type-Specific Ca2+ Current Profiles. *Journal of Neurophysiology*, 102(5), pp.2834–2845. Available at: http://jn.physiology.org/content/102/5/2834.full-text.pdf+html [Accessed September 2, 2014].

Ito, K. et al., 2014. A systematic nomenclature for the insect brain. *Neuron*, 81(4), pp.755–65. Available at: http://www.sciencedirect.com/science/article/pii/S0896627313011781 [Accessed July 11, 2014].

Kloppenburg, P. et al., 1999. Dopamine Modulates Two Potassium Currents and Inhibits the Intrinsic Firing Properties of an Identified Motor Neuron in a Central Pattern Generator Network Dopamine Modulates Two Potassium Currents and Inhibits the Intrinsic Firing Properties of an Identi. , pp.29–38.

Kloppenburg, P., Kirchhof, B.S., et al., 1999. Voltage-Activated Currents From Adult Honeybee (Apis mellifera) Antennal Motor Neurons Recorded In Vitro and In Situ Voltage-Activated Currents From Adult Honeybee (Apis mellifera) Antennal Motor Neurons Recorded In Vitro and In Situ. , pp.39–48.

Kloppenburg, P., Ferns, D. & Mercer, a R., 1999. Serotonin enhances central olfactory neuron responses to female sex pheromone in the male sphinx moth manduca sexta. *The Journal of neuroscience : the official journal of the Society for Neuroscience*, 19(19), pp.8172–81. Available at: http://www.ncbi.nlm.nih.gov/pubmed/10493719.

Liu, Y.-H. & Wang, X.-J., 2001. Spike-Frequency Adaptation of a Generalized Leaky Integrate-and-Fire Model Neuron. *Journal of Computational Neuroscience*, 10(1), pp.25–45. Available at: http://link.springer.com/article/10.1023/A:1008916026143 [Accessed September 27, 2014].

Miller, M.N., Okaty, B.W. & Nelson, S.B., 2008. Region-specific spike-frequency acceleration in layer 5 pyramidal neurons mediated by Kv1 subunits. *The Journal of neuroscience : the official journal of the Society for Neuroscience*, 28(51), pp.13716–26. Available at: http://www.pubmedcentral.nih.gov/articlerender.fcgi?artid=2677066&tool=pmcentrez&rendertype=abstract [Accessed September 11, 2014].

Peron, S.P. & Gabbiani, F., 2009. Role of spike-frequency adaptation in shaping neuronal response to dynamic stimuli. *Biological cybernetics*, 100(6), pp.505–20. Available at: http://www.pubmedcentral.nih.gov/articlerender.fcgi?artid=2854487&tool=pmcentrez&rendertype=abstract [Accessed September 27, 2014].

Powers, R.K. et al., 1999. Multiple mechanisms of spike-frequency adaptation in motoneurones. *Journal of Physiology-Paris*, 93(1-2), pp.101–114. Available at: http://www.sciencedirect.com/science/article/pii/S0928425799801417 [Accessed September 26, 2014].

Sah, P. & Davies, P., 2000. Calcium-Activated Potassium Currents In Mammalian Neurons. *Clinical and Experimental Pharmacology and Physiology*, 27(9), pp.657–663. Available at: http://doi.wiley.com/10.1046/j.1440-1681.2000.03317.x [Accessed September 27, 2014].

Shang, Y. et al., 2007. Excitatory local circuits and their implications for olfactory processing in the fly antennal lobe. *Cell*, 128(3), pp.601–12. Available at: http://www.pubmedcentral.nih.gov/articlerender.fcgi?artid=2866183&tool=pmcentrez&rendertype=abstract [Accessed September 28, 2014].

Sobel, E.C. & Tank, D.W., 1994. In vivo Ca2+ dynamics in a cricket auditory neuron: an example of chemical computation. *Science (New York, N.Y.)*, 263(5148), pp.823–6. Available at: http://www.ncbi.nlm.nih.gov/pubmed/17770837 [Accessed September 27, 2014].

Stocker, M., 2004. Ca(2+)-activated K+ channels: molecular determinants and function of the SK family. *Nature reviews. Neuroscience*, 5(10), pp.758–70. Available at: http://www.nature.com/nrn/journal/v5/n10/execsumm/nrn1516.html [Accessed August 27, 2014].

Stopfer, M. et al., 1997. Impaired odour discrimination on desynchronization of odour-encoding neural assemblies. *Nature*, 390(6655), pp.70–4. Available at: http://www.ncbi.nlm.nih.gov/pubmed/9363891 [Accessed September 17, 2014].

Strausfeld, N.J. & Hildebrand, J.G., 1999. Olfactory systems: common design, uncommon origins? *Current opinion in neurobiology*, 9(5), pp.634–9. Available at: http://www.ncbi.nlm.nih.gov/pubmed/10508748 [Accessed September 29, 2014].

Sun, X.J., Tolbert, L.P. & Hildebrand, J.G., 1997. Synaptic organization of the uniglomerular projection neurons of the antennal lobe of the moth Manduca sexta: a laser scanning confocal and electron microscopic study. *The Journal of comparative neurology*, 379(1), pp.2–20. Available at: http://www.ncbi.nlm.nih.gov/pubmed/9057110 [Accessed September 28, 2014].

Vosshall, L.B., Wong, A.M. & Axel, R., 2000. An Olfactory Sensory Map in the Fly Brain. *Cell*, 102(2), pp.147–159. Available at: http://www.sciencedirect.com/science/article/pii/S0092867400000210 [Accessed September 28, 2014].

Wilson, C.J. et al., 2004. A model of reverse spike frequency adaptation and repetitive firing of subthalamic nucleus neurons. *Journal of neurophysiology*, 91(5), pp.1963–80. Available at: http://jn.physiology.org/content/91/5/1963.full-text.pdf+html [Accessed September 27, 2014].

Wilson, R.I. & Laurent, G., 2005. Role of GABAergic inhibition in shaping odor-evoked spatiotemporal patterns in the Drosophila antennal lobe. *The Journal of neuroscience : the official journal of the Society for Neuroscience*, 25(40), pp.9069–79. Available at: http://www.jneurosci.org/content/25/40/9069.short [Accessed July 28, 2014].

Eidesstattliche Erklärung

Ich erkläre hiermit, dass ich diese Bachelorarbeit selbstständig, ohne Hilfe Dritter und ohne Benutzung anderer als den angegebenen Quellen und Hilfsmitteln verfasst habe. Alle benutzten Quellen, wörtlich oder sinngemäß entnommene Stellen, sind als solche einzeln kenntlich gemacht.

Diese Arbeit ist bislang keiner anderen Prüfungsbehörde vorgelegt worden und auch nicht veröffentlicht worden.

Ich bin mir bewusst, dass eine falsche Erklärung rechtliche Folgen haben wird.

Köln, den _____

Unterschrift

Danksagung

Zuallererst möchte ich Herrn Prof. Dr. Peter Kloppenburg für die großartige Möglichkeit danken, meine Bachelorarbeit in seiner Arbeitsgruppe schreiben zu dürfen. In vielen persönlichen Gesprächen wusste er mit gutem Rat die Arbeit in die richtigen Bahnen zu lenken. Auch Herrn PD Dr. Joachim Schmidt danke ich für die Zweitkorrektur meiner Arbeit

Weiterhin gilt natürlich ein großer Dank den Mitgliedern der AG Kloppenburg, die mich in den letzten Monaten ertragen haben und sich trotz all der vergossenen (Wut) - Tränen um mich und meine Anliegen gekümmert haben. Hier besonderer Dank an Sandra, Ursel und Viktor: ihr habt auch an Wochenenden noch nicht genug von mir gehabt! Der freundschaftliche Umgang innerhalb der gesamten Mannschaft war großartig und hat die vielen Arbeitsstunden nicht immer wie Arbeit wirken lassen.

Der größte Dank gilt natürlich meiner Familie aber insbesondere meinen lieben Eltern. Ihr habt diese lange Zeit meines bisherigen Studierens möglich gemacht, mich unterstützt wo ihr nur konntet und mir in all der Zeit größten Rückhalt gegeben.

Danke!